UNIVERSITY OF ANTIOQUIA

Mass Modelling of Globular Clusters in the Milky Way

by

Juan Manuel Espejo Salcedo

Advisor:

Juan Carlos Muñoz Cuartas

A thesis submitted in partial fulfillment for the degree of Astronomer

in the

Natural Sciences Faculty

Institute of Physics

October 2015

"We are just and advanced breed of monkeys on a minor planet of a very average star. But we can understand the Universe. That makes us something very special."

Stephen Hawking

Abstract

Natural Sciences Faculty
Institute of Physics

The study of the dynamics and mass modelling of galaxies is a very complex but beautiful branch of modern Astrophysics and Cosmology. When you follow this route it is perhaps inevitable the need of studying stellar sytems inside galaxies because they are inherent all along the way of the history and the formation and structure of galaxies themselves. This thesis work is intended to show our work on mass models of Globular Clusters in the Milky Way with our own data obtained in OPD observatory. By using spectra of the central region of the clusters we compute radial velocities of the stars to obtain information about the velocity dispersion profile thus obtaining information about the potential well responsible for the dynamics of those individual stars. With this information, aside the mass estimations given by the photometry results we can build mass models of the clusters looking for insight on the amount of dark matter present in this kind of structures, if dark matter is present at all…

Acknowledgements

The acknowledgements and the people to thank go here, don't forget to include your project advisor…

Contents

Abstract ii

Acknowledgements iii

List of Figures vi

List of Tables vii

1 Introduction 1

2 Theoretical Framework 4
- 2.1 Globular Clusters . . . 4
  - 2.1.1 Basics . . . 5
  - 2.1.2 Formation and evolution . . . 7
  - 2.1.3 Observational Properties . . . 11
- 2.2 Mass models and Dynamics . . . 15
  - 2.2.1 Potential Theory of Spherical Systems . . . 15
  - 2.2.2 Collisionless Systems . . . 20
  - 2.2.3 Dynamics . . . 22
- 2.3 Scenario and Observations . . . 25
- 2.4 Simulations . . . 26

3 Observations and Analysis 29
- 3.1 Observational Procedures . . . 29
  - 3.1.1 Spectroscopic Data . . . 30
  - 3.1.2 Photometric Data . . . 32
- 3.2 First step for Anaysis . . . 33
- 3.3 Photometry . . . 34
  - 3.3.1 Aperture Photometry . . . 36
  - 3.3.2 PSF Photometry . . . 38
- 3.4 Spectroscopy . . . 40
  - 3.4.1 Spectroscopic Reduction . . . 41
  - 3.4.2 Extraction . . . 42
  - 3.4.3 Wavelength Calibration . . . 44
  - 3.4.4 Flux Calibration . . . 45

3.5 RVSAO and radial velocity determination 48

4 Modelling **50**

5 Conclusions **51**

Bibliography **52**

List of Figures

2.1 M15 Globular Cluster 5
2.2 ESO and Hubble images of Globular Clusters 6
2.3 Evolution of an ergodic Plummer model over time 10
2.4 Evolution of the velocity anisotropy parameter 11
2.5 Color Magnitude diagram of M55 12
2.6 Age vs Metallicity for some Globular Clusters 13
2.7 Illustration of the orbits of Globular Clusters around a spiral galaxy . . . 14
2.8 Spectral line broadening 15
2.9 Circular speed vs radius for the Jaffe, Hernquist, and NFW models 20
2.10 Galaxy merger model 1m11 from Kruijssen et al. (2012b) 28

3.1 OPD Observatory 30
3.2 Perkin-Elmer telescope used for Spectroscopy 30
3.3 IAG Telescope used for Photometry 32
3.4 Dirty image of NGC5139 35
3.5 Clean image of NGC5139 35
3.6 Normalized Superflat for the filter I 36
3.7 NGC5139 as observed in the V filter 37
3.8 Photometry results of Magnitudes vs Size of apertures 38
3.9 PSF modelling 39
3.10 PSF residuals 40
3.11 PSF image created by the task Seepsf 40
3.12 Dirty spectrum of NGC5139 42
3.13 Clean spectrum of NGC5139 42
3.14 Spectrum of calibration star HR4468 43
3.15 Emission lines for the Ne-Ar calibration lamp 44
3.16 Theoric emisison lines of a Ne-Ar lamp 44
3.17 Wavelength calibrated spectrum of HR4468 45
3.18 Flux calibrated spectrum of HR4468 47
3.19 Spectrum of a prominent star of the NGC5139 globular cluster 48
3.20 The nature of the barycenter shift of radial velocities 49

List of Tables

2.1 Summary chart of Star Clusters 7
2.2 Two power density potentials 19

3.1 Observed objects in OPD 31

For/Dedicated to/To my…

Chapter 1

Introduction

As the oldest known subunits of our Galaxy, Globular Clusters are the primary "fossils" from its early evolution, and they may hold the key to understanding its formation. For example, the amount of dark matter that they could (or not) have may be an important clue to the understanding of the formation of the Milky Way. Despite the large amount of observational data and the advances in theoretical work, still, there is not yet a convincing model to describe the formation of these ancient structures.

Two broad types of possibilities have been considered: one is that the globular clusters were the very first condensed systems to form in the early universe, and the second is that they originated in larger star-forming systems that later merged to form the present galaxies.

The first possibility includes the suggestion of Peebles & Dicke (1968) that the globular clusters were formed by Jeans fragmentation in the early universe, this possibility is in concordance with the current scenario of galaxy formation in which galaxies are formed inside the deepest regions of the gravitational potential well provided by dark matter halos. This explanation has been received with great interest by the scientific community since it not only fits within the hierarchical scenario of structure and galaxy formation, but also may help to understand some of the open problems in the standard model, such as the abundance of low mass structures (Klypin et. al. 1999). However, evidence has been found against this scenario. For example, Odenkirchen et al. (2003) have found tidal tails surrounding globular clusters, something that is not expected if globular clusters form and reside inside extended dark matter halos.

Regarding the second possibility, Fall & Ries (1985, 1988) proposed the formation of globular clusters as a response to thermal instabilities in the hot gaseous halos of massive galaxies. The Fall & Rees hypothesis has been popular among theorists who have used it to predict the characteristic properties of globular clusters, although it has proven difficulties to justify the assumed thermal behaviour of the cluster-forming gas clouds. This scenario presents a problem since there are observations that suggest that very low mass galaxies, not massive enough to host a hot gaseous halo, may also have their own globular clusters.

Not only the formation of these structures is puzzling, their composition is also a challenging problem because some authors say that these structures do not contain any dark matter contributions and that their gravitational stability can be explained completely with the baryonic matter inside of them. Conroy et. al. (2011) have used density profiles to argue against the presence of dark matter inside globular clusters, while Ibata et. al. (2013) have found that under general conditions it could be possible to find significant fractions of dark matter in globular clusters. Modelling the mass content of globular clusters in the galaxy would help to disentangle the mechanism driving its formation process. Mass modelling would allow to study the mass distribution in the inner region of globular clusters, determining the dominant components (Breddels M. A. et.al. 2013, Adams J. J. et. al., 2012, van den Bosch R.C.E. et. al. 2006) providing light on the problem of the origin of globular clusters.

Our aim in this project is to build our own mass model for the Globular Clusters using some data observed in OPD observatory in May 2014 so that we can be able to discuss and find new evidence on the existence or absence of dark matter in them according to these results.

With our set of data, we do the preliminary reduction and analysis of photometric and spectroscopic data, including the wavelength and flux calibration of the spectra. The photometric data will show us the mass to light ratio of the Globular Clusters thus giving us information about the baryonic mass content of the clusters. On the other hand, the spectroscopic data will give us information about the radial velocity of the stars that will provide us the statistical dispersion of velocities in the inner region of the clusters thus giving us information about the potential well in the clusters. This procedure is done using the Radial Velocity Package of IRAF called *RVSAO* which uses cross correlation techniques in the Fourier transform of templates and scientific spectra to infer the doppler broadening of the emission and/or absorption lines in our data and allows us to calculate their radial velocities.

After this analysis has been made upon all the observational data we can start the theoretical analysis including simulations of N-body systems and study of the initial conditions that will preserve the spherical symmetry of the clusters, taking into account our results on the dominant components of the clusters.

The bulk properties of GCs, with the possible exception of their innermost regions, can be modelled using the collisionless Boltzmann equation (Binney & Tremaine 1987), from which the statistical properties of the velocity distribution of stars can be derived. In particular, one can derive a formulation for the velocity dispersion tensor that, in the isotropic, non rotating case, reduces to a scalar quantity. This quantity can be determined using the appropriate Jeans equation. This calculation requires knowledge of the distribution function (DF) that determines the number of stars in a given region of space, and the gravitational potential.

The best fit for our data with the theoretical assumptions will tell us how mass is distributed in the clusters and it will allow us to conclude if there is a significant contribution of dark matter to the potential well that provides the stars the observed velocities. As mentioned before, the Mass Modelling will let us have a good insight into the problem of the formation of these structures.

Chapter 2

Theoretical Framework

Typical galaxies all around the Universe hold different structures such as stellar systems of between 10^2 and 10^6 stars which orbit their galactic core . We call these interesting systems star clusters and they are basically divided into three main types: Open Clusters, stellar associations and **Globular Clusters**. Open clusters are stellar systems that can contain from hundreds to thousands of stars, they are formed continuously in the Galactic disk and most of them are relatively young (younger than 1 Gyr). Old open clusters are rare since their gravitational stability is very low and can be easily disrupted by gravitational shocks from passing interstellar gas clouds. It seems likely that most of the stars in the galactic disk were formed in open clusters that have dissolved since then.

Stellar associations such as young associations of stars that can contain 10100 massive stars of spectral class O and B, and are known as OB associations. These associations also contain hundreds or thousands of low- and intermediate-mass stars.

Globular clusters, the other important class of stellar systems, are much more interesting and we focus deeply on their properties and characteristics.

2.1 Globular Clusters

Globular clusters are very massive stellar systems that can contain from thousands to millions of stars in a nearly spherical distribution spread over a volume of several tens to about 200 light years in diameter. These stellar systems are composed of old stars and they do not contain gas or dust. As an example the next figure shows M15 Globular Cluster, that was discovered by Jean-Dominique Maraldi in 1746 while he was studying the De Chseaux comet.

FIGURE 2.1: Globular Cluster M15, taken by the Hubble Space Telescope with an exposition time of 900 seconds. Image by NASA

Let's discuss in further the details of these systems.

2.1.1 Basics

A Globular Cluster is a compact, gravitationally bound group of hundreds of thousands to several million stars that are themselves gravitationally bound to galaxies. They have comparable ages to their associated galaxies which is an encouraging characteristic to study them as they could provide valuable information about the formation and evolution of their host galaxies.

Their star populations are uniformly old, although different stellar populations are found as we improve our measurements and observations. Globular clusters are devoid of gas so that pretty much no new stars form in them. The stars at the centre of a globular cluster are much more densely packed than the stars in other parts of the galaxy.

Globular clusters revolve about the nucleus of a galaxy on orbits of high eccentricity and high inclination to the galactic plane. About a third of globular clusters are concentrated around the galactic center. A typical cluster has a period of revolution around the order of 10^8 years. A cluster spends most of its time far from the center of a galaxy, and so most of them can, and have been discovered in the spaces between galaxies.

Due to clusters moving in various orbits in the Galaxy, they are bound together with gravitational forces that are stronger than the disrupting forces exerted on it by the Galaxy or other nearby stars, and this results in an added condition for the stability of a cluster.

The spherical shape of these systems is due to the reached stability that they can acquire over time. To ensure the stability of an isolated cluster, the average speed of its individual stars must not exceed the escape velocity from the cluster. If this occurred, the stars would escape into space, and the cluster would dissipate. If the stellar velocities are low enough to satisfy this condition, then the cluster is gravitationally bound, i.e. the force of gravity is strong enough to keep the member stars from escaping.

Another factor in the stability of clusters is size; the smaller and more compact the cluster, the greater its own gravitational binding force compared with the disrupting forces, and the more chance it has to survive to old age.

Because globular clusters are highly compact systems, they are consequently very stable, and so most globular clusters will probably maintain their identity almost indefinitely. But even these clusters lose some stars, especially if they have a low mass. This is due to there always being a few stars in a cluster that move faster than the cluster's average speed.

When a star escapes, it carries with it energy, removing this energy from the cluster as a whole. This eventually results in the cluster developing a tightly bound core surrounded by a rarefied halo of stars as we can see in the following images of Globular Clusters:

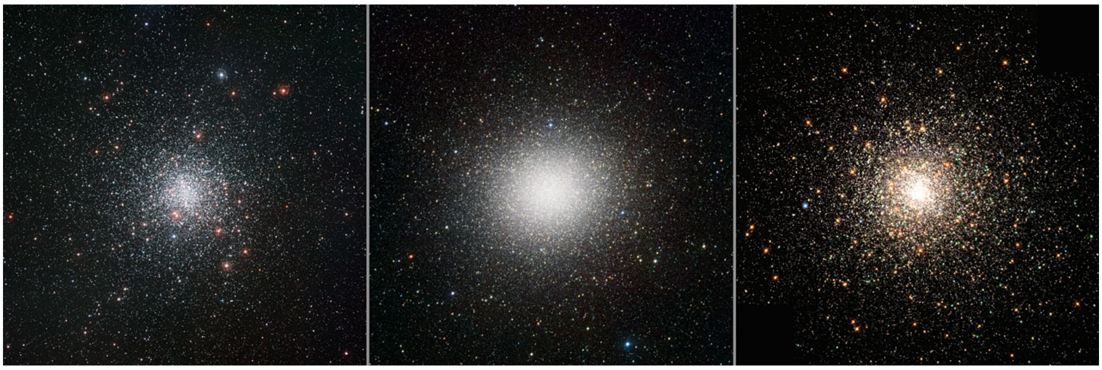

FIGURE 2.2: Globular Clusters taken by ESO and the HST. From left to right: M4 (ESO), Omega Cen (ESO) and M80 (Hubble). Image from the Hubble Space Telescope database.

In the dense core of a cluster, the stars occasionally collide, and some of the debris eventually coalesces. Predictions indicate that this dynamical evolution could lead to the development of a large Black Hole at the cluster's center. At the same time, a few stars in the outer parts of the cluster would continue to escape. The escape rate and dynamical evolution for the rich globular clusters are so slow that the clusters can easily survive for many billions of years, remaining mostly unchanged.

Observations and mass models of these structures show that the average star density in a Globular Cluster is about 0.4 stars per cubic parsec. In the dense center of the cluster, the star density can increase from 100 to 1000 per cubic parsec, as we shall discuss in another section. However, even in the center of clusters, there is still plenty of space between the stars.

In order to understand how dense Globular Clusters can be, we may think of a clear example like Proxima Centauri, which is 4.2 light-years, or about 1.3 parsecs from Earth. Thus, if we were able to draw a sphere around the Sun with a radius of 1.3 parsecs, it would only contain 2 stars: the Sun and Proxima Centauri. But if you were to draw this same sphere in the center of the globular cluster M13, it would contain approximately 10,000 stars.

To summarize and compare some of the main characteristics we just mentioned about globular clusters with other stellar systems let's see the following table:

Characteristic	**Open Custers**	**OB Associations**	**Globular Clusters**
Diameter (pc)	< 10	$30 - 200$	$20 - 100$
Number of Stars	$50 - 1000$	$10 - 100$	$10^4 - 10^6$
Mass ($M_\odot$)	$100 - 1000$	$100 - 1000$	$10^4 - 10^6$
Density ($M_\odot/pc^3$)	$0.1 - 10$	< 0.01	$0.5 - 1000$
Shape	Irregular	Irregular	Spherical
Color (Common)	Red or Blue	Blue	Red
Metallicity	High	High	Low
Location	Disk of Galaxy	Disk of Galaxy	Halo of Galaxy

TABLE 2.1: Summary chart of Star Clusters, taken from http://astronomyonline.org

2.1.2 Formation and evolution

The formation of Globular Clusters is not well understood yet, and we only have crude ideas of their typical states right after they have reached the dynamical equilibrium.

As it was mentioned in the introduction, two main broad types of possibilities have been considered to explain the very first processes that created these structures. The first one suggests that in the early universe the first structures that came to exist were globular clusters by Jeans Fragmentation. One of the main contributions to this possibility was given by Peebles & Dicke (1968) who first pointed out that globular clusters might have formed even before the collapse of the protogalaxy, noting the fact that the baryonic Jeans mass right after decoupling is about the size of a Globular Cluster. Although their possibility is in concordance with the current scenario of galaxy formation in which galaxies are formed inside the deepest regions of the gravitational potential well provided by dark matter halos, there are still problems of this theory, for example, it cannot explain why there are so few intergalactic globular clusters and why the properties of globular clusters are correlated with their host galaxies.

Another problem with this theory is some observational results like the ones found by Odenkirchen et al. (2003) who found tidal tails surrounding globular clusters. This is not expected if globular clusters form and reside inside extended dark matter halos that would keep the stability and thus avoiding the creation of these tidal tails.

The second possibility suggests that the formation of Globular clusters was a response to thermal instabilities present in large hot halos of massive galaxies full of gas. In their model, cold dense clouds condense out of hot and tenuous background to form as progenitors of globular clusters. This idea corresponds to the late-forming theory Globular Clusters that could be in accordance with the present observational properties of Globular Clusters like their characteristic metallicity, but it has proven difficulties to justify the assumed thermal behaviour of the cluster-forming gas clouds. Also, there are observations that suggest that very low mass galaxies, not massive enough to host a hot gaseous halo, may also have their own globular clusters.

Many theories on Globular Cluster formation assume a smooth and rapid collapse of the protogalaxy (Eggen, Lynden-Bell, & Sandage 1962) but some other authors (Searle & Zinn 1978) state that the early Galactic environment migth have been much more chaotic and violent.

Murray & Lin (1992) have argued that self-gravitating clouds are unstable to fragmentations and spontaneous star formation so that globular clusters must form from sub-Jeans mass clouds. In subsequent work Murray et al. (1993) have shown that only clouds in a limited mass range ($10^4 M_\odot \lesssim M \lesssim 10^6 M_\odot$) can survive both the Kelvin-Helmholtz instability and the thermal instability which does not lead to bound clusters. Clouds within the critical mass range will form globular clusters if they are induced into cooling and collapse by collisions of sufficient velocity.

Mathews & Schramm proposed a schematic merger model for the formation of the halo and chemical evolution of the Galaxy in which the protogalaxy forms by mergers of small subgalactic gas clouds. This merger model, as discussed by Lee, Schramm & Mathews 1994 could also be a possible scenario for Globular Clusters formation.

Moving on to the evolution of these systems, we note that our current observations and modelling give us good results after the equilibrium has been reached, in this context, there must be mentioned that the mechanism that drives the system to stability is relaxation. This proccess pretty much erases the cluster's memory of it's initial state so the results for gravitational stable systems can be reached using a wide range of initial conditions.

Since the relaxation time is inversely proportional to density evolution due to relaxation proceeds most rapidly in the dense central regions of the clusters. Within this central region that is relaxed, the distribution function f and the density distribution should be approximate to a isothermal distribution, this means that the distribution function must be approximately Maxwellian at energies well bellow the escape energy. We asume that in the outer parts of the clusters the relaxation time is long and encounters have relatively little effect.

Other important characteristic of their evolution is they lose mass from stellar evolution: Our stellar evolution theories show us that stars often eject mass from their surfaces near the ends of their lives. For the mass-losing stars inside globular clusters, the ejected mass is likely to escape the cluster, either because the ejection velocity exceeds the escape speed from the cluster or because it interacts with the galactic gas when the cluster is passing throw the disk. So we conclude that the clusters lose mass as stars evolve. It must be mentioned that the evolution timescale of a typical population of stars is usually much longer than the crossing time in the cluster.

The mass lost by a cluster due to stellar evolution depends on the initial mass function which specifies the distribution of masses of stars just after they have formed and the initial-final mass function.

Now, when we talk about the evolution of the Globular Clusters, we must see how the mass distribution evolves over time. the evolution of the mass distribution in an isolated cluster, that began as a Plummer model (that we shall introduce in the following section) is shown in the next figure:

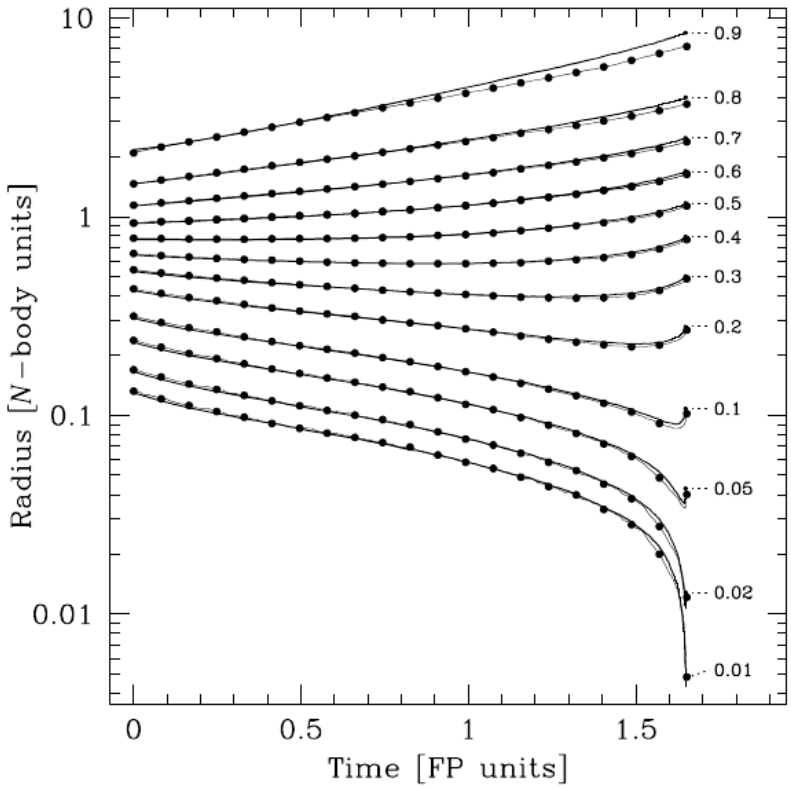

FIGURE 2.3: Evolution of an ergodic Plummer model, according to an orbit-averaged Monte-Carlo solution of the Fokker Planck equation with 3×10^5 superstars (heavy solid lines) and an N-body simulation with 65536 superstars (dots, connected by solid lines). From Freigat, Rasio, & Baumgardt (2006)

As we can see above, the outer half of the cluster expands, mainly due to the gradual growth of the halo as stars in the core diffuse towards the escape energy. But most importantly, we can see that the center contracts, this process is known as **core collapse** and it leads to a dramatic growth in the central density that may indicate the existence of an apparent singularity in the central density.

By solving the orbit-averaged Fokker-Planck equation for an isolated, spherical cluster (without binaries) and starting from a Plummer model, Takahashi (1995) found a more accurate calculation of core collapse. His calculations allow greater dynamic range than Monte Carlo or N-body methods. His results show that as the cluster evolves, the core radius shrinks and the central density grows. Outside the core, the density profile approaches a power law $\rho \propto r^{-2.23}$.

Another interesting result regarding the direct solutinos of the orbit-avergaed Fokker Planck equations is the behaviour of the anisotropy parameter $\beta = 1 - \overline{v_\theta^2}/\overline{v_r^2}$ as we can see in the following figure:

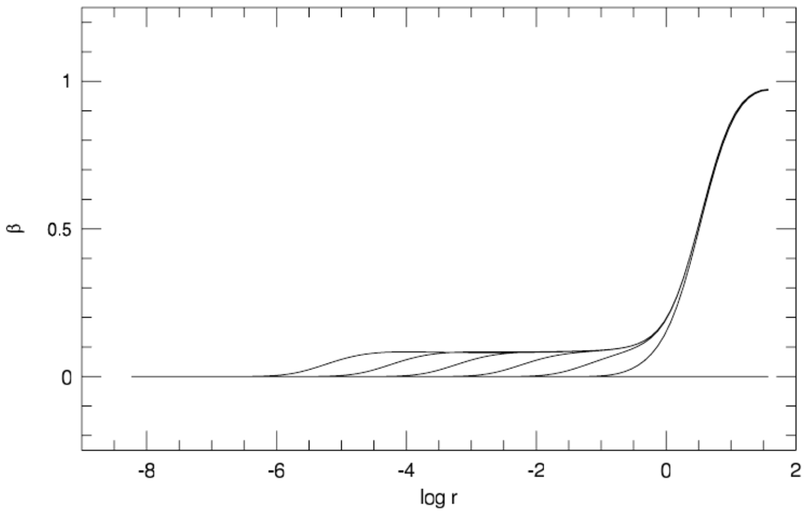

FIGURE 2.4: The evolution of the velocity anisotropy parameter for an orbit-averaged Fokker Planck calculation of core collapse. From Takahashi (1995)

At large radii, the anisotropy parameter (that indicates the tendency of the system to have or not preferred directions) tends to unity ($\beta \simeq 1$), and that indicates that the orbits are nearly radial, at the smalest radii, inside the shrinking core, we have $\beta \simeq 0$, which indicates that the velocity distribution is isotropic. We note that in the radius range in which the density profile in the top panel is a power law, there is a constant small radial anisotropy of $\beta \simeq 0.08$ or $\overline{v_\theta^2}/\overline{v_r^2} \simeq 0.92$

Regarding the late interactions and accretion processes, we note that although our Galaxy has evidently not experienced any further major accretion events capable of disrupting the disk, it is possible that minor accretion events affecting only the halo and not the disk have continued to occur (Navarro, Frenk, & White 1994), but their net effect on the GC's dynamics and stability is the context of cosmology is very low.

The evolution process for these systems are so long that this fit entirely in the context of Cosmology. Most of the clusters whose masses are larger than $10^5 M\odot$ have lifetimes longer than the Hubble time.

2.1.3 Observational Properties

Globular clusters were once thought to consist of a single population of stars that all formed together. However, research has since shown that many of the Milky Way's globular clusters had far more complex formation histories and are made up of at least two distinct populations of stars.

A way of analysing the stellar populations in Globular Clusters is to use Colour-Magnitude diagrams. A colour-magnitude diagram is a plot of the apparent magnitudes of the stars in a cluster against their colour indices. Globular Clusters nearly all have very similar colour-magnitude diagrams.

This diagram for a typical globular cluster looks very different than that of an open cluster. There are no Main Sequence stars of types OBAF, but there are many red giants. The brightest stars in a globular cluster are those at the tip of the red giant branch in the color-magnitude diagram, which explains the red appearance of the bright stars in color images of the clusters. You can also see stars populating the horizontal branch (and also why it is called the horizontal branch), the asymptotic giant branch, and even some stars that have colors and magnitudes of F stars, but far fewer than the G stars just below and to the right of them on the Main Sequence. As we can see in the following figure:

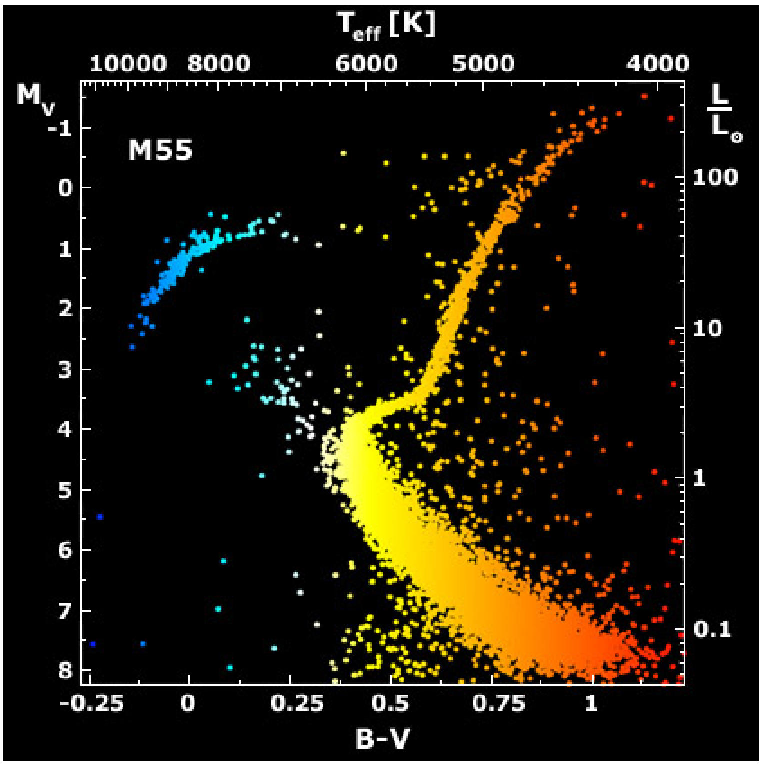

FIGURE 2.5: Color Magnitude diagram of M55. Image by NASA

Of these populations, around half the stars are a single generation of normal stars that were thought to form first, and the other half form a second generation of stars, which are polluted with different chemical elements. In particular, the polluted stars contain up to 50100 times more nitrogen than the first generation of stars.

The proportion of polluted stars found in the Milky Way's globular clusters is much higher than astronomers expected, suggesting that a large chunk of the first-generation star population is missing. A leading explanation for this is that the clusters once contained many more stars, but a large fraction of the first-generation stars were ejected from the cluster at some time in its past.

An interesting plot relating the age of the Globular Clusters to their metallicity is shown in the following figure:

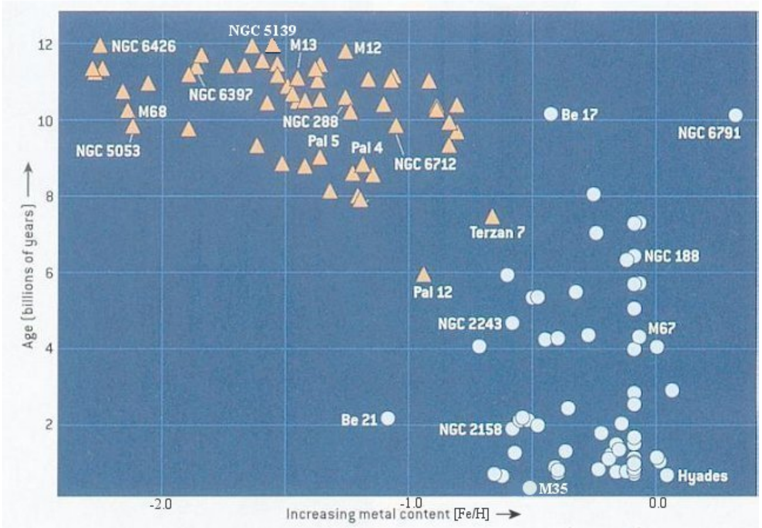

FIGURE 2.6: Age estimations vs metallicity of Open (circles) and Globular (triangles) Clusters. Taken from https://universe-review.ca

Before now, we didn't know whether globular clusters in smaller galaxies had multiple generations or not, but our observations show clearly that they do. This finding means that a leading theory on how these mixed-generation globular clusters formed cannot be correct, and astronomers will have to think once more about how these mysterious objects in the Milky Way and further afield came to exist.

The other fundamental observational procedures to study GC's are Radial velocity measurements that have revealed that most Globular Clusters are moving in highly excentric elliptical orbits that take them far outside the Milky Way; they form a halo of roughly spherical shape which is highly concentrated to the Galactic Center, but reaches out to a distance of several 100,000 light years, much more than the dimension of the Galaxy's disk. As they don't participate in the Galaxy's disk rotation, they can have high relative velocities of several 100 km/sec with respect to our solar system; this is what shows up in the radial velocity measurements. Ninkovic (1983) has estimated eccentricities of globular cluster orbits. Cudworth and Hanson (1993) undertook some first rough determinations of proper motions with respect to background galaxies. From these and similar measurements, Van den Bergh (1995) estimated perigalactic distances, and Dauphole et.al. (1996) calculated first approximate orbits. Much more acurate data for proper motions became only available from astrometrical data obtained with ESA's Hipparcos satellite in 1997, from which space motions (Geffert et.al. 1997) and approximate orbits (Brosche et.al. 1997) could be determined.

We can visualize their orbits in the following figure:

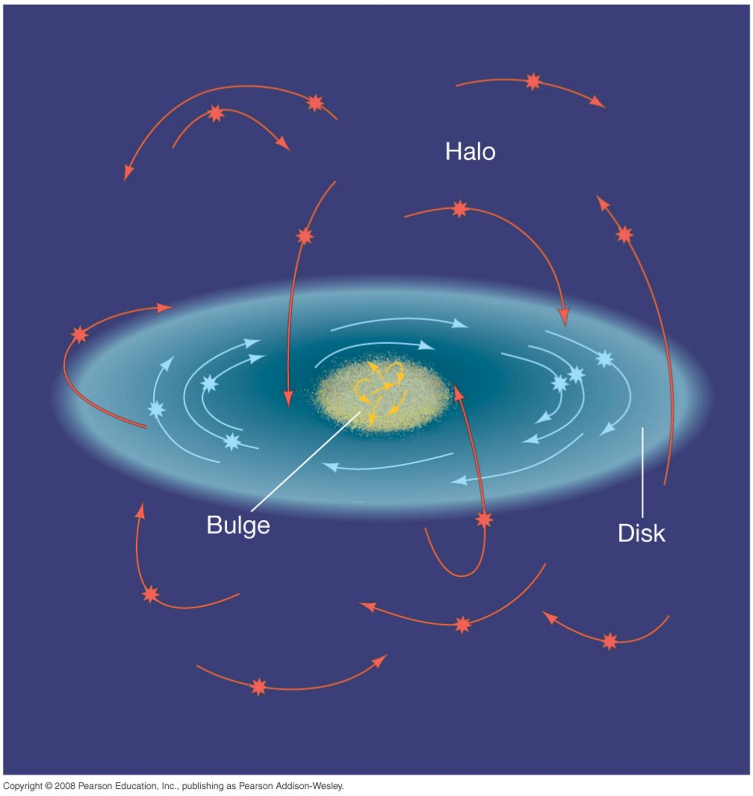

FIGURE 2.7: Illustration of the orbits of some Globular Cluster in a spiral galaxy like the Milky Way. Picture from the Oregon University webpage

To determine the physical orbits of stars in globular clusters, it is required to know their proper motions in addition to their radial velocities. This can be achieved by measuring the doppler broadening of the spectral lines in the clusters as we can see in the following figure

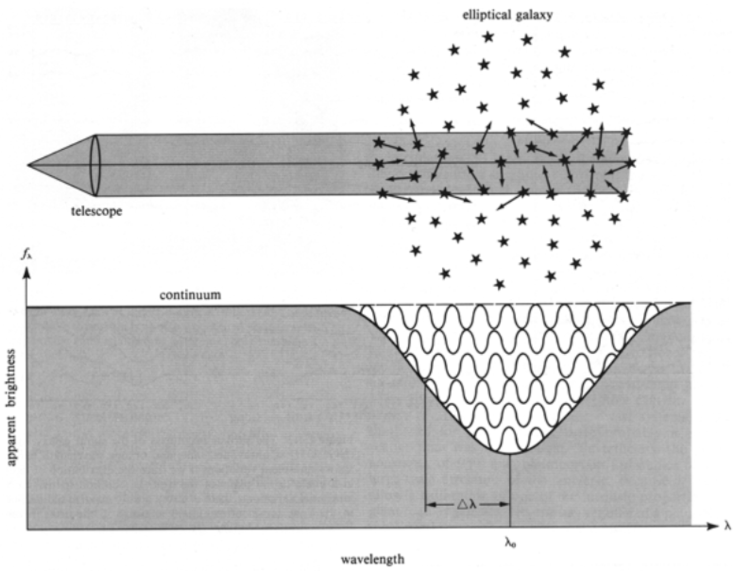

FIGURE 2.8: Observed spectral line broadening due to the proper motions of stars in the cluster, note that the observed $\Delta\lambda$ is given by the blue shift or red shift of each individual star contributing to the broadening of the line, this gives important information about the velocity dispersion that will be discussed in a following section. Taken from lecture notes of the University of Arizona

We will study further the mass models that fit best to Globular Clusters and the dynamical structure in the following section.

2.2 Mass models and Dynamics

In order to get into the physical discussions about the stability and modelling of globular clusters, we need to understand first the basics of potential theory, and more specifically the potential theory of spherical systems. The next step is to discuss the physical implications behind these models so that the mass modelling can be made. The last but most important part is to discuss the criteria regarding the mathematical treatment of the dynamics of these systems in the context of the collisionless Boltzmann equation and the approximations to the solutions of the Jeans equations that will be used for the fitting of the observational data to do the final modelling.

2.2.1 Potential Theory of Spherical Systems

Our discussions about Potential Theory for large stellar systems will be studied using the simplifications given by the spherical symmetry of globular clusters. We first introduce some of the most important theorems for calculating the gravitational potential of an spherically symmetric distribution of matter provided by Newton, these theorems are physically related to Gauss theorem and may be proved using simple geometric assumptions or using a more precise results from vectorial calculus.

Newton's first theorem states that a body that is inside a spherical shell of matter experiences no net gravitational force from that shell.

Newton's second theorem states that the gravitational force on a body that lies outside a sphericall shell of matter is the same as it would be if all the shell's matter were concentrated into a point at its center.

It follows from Newton's theorems that the gravitational attraction of a spherical density distribution $\rho(r')$ on a unit mass at radius r is entirely determined by the mass interior to r:

$$\mathbf{F}(r) = -\frac{GM(r)}{r^2}\hat{\mathbf{e}}_r \tag{2.1}$$

Where the mass as a function of the radius is

$$M(r) = 4\pi \int_0^r dr' r'^2 \rho(r') \tag{2.2}$$

We can consider that the total gravitational potential of the spherical system is the sum of the potentials given by spherical shells of a diferential mass $dM(r) = 4\pi\rho(r)r^2dr$. This way, we may calculate the gravitational potential at $\mathbf{r}$ generated by a spherically symmetruc density distribution $\rho(\mathbf{r}'$ by adding the contributions to the potential produced by shells with $r' < r$, and with $r' > r$. Thus we obtain:

$$\begin{aligned} \Phi(r) &= -\frac{G}{r}\int_0^r dM(r') - G\int_r^\infty \frac{dM(r')}{r'} \\ &= -4\pi G\left[\frac{1}{r}\int_0^r dr' r'^2\rho(r') + \int_r^\infty dr' r'\rho(r')\right] \end{aligned} \tag{2.3}$$

We note an important property of a spherical matter distribution regarding its circular speed $v_c(r)$, defined to be the speed of a particle of negligible mass in a circular orbit at radius r. We may evaluate v_c by equating the gravitational attraction $|\mathbf{F}|$ to the centripetal acceleration ${v_2}^2/r$:

$$v_c^2 = r|\mathbf{F}| = r\frac{d\Phi}{dr} = \frac{GM(r)}{r} \tag{2.4}$$

We may also note that the **escape speed** v_e in terms of the gravitational potential is:

$$v_e(r) \equiv \sqrt{2|\Phi(r)|} \tag{2.5}$$

The **potential energy of spherical systems** comes from a very general equation, also in terms of the potential:

$$W = -\int d^3x\rho x \cdot \nabla\Phi \tag{2.6}$$

By substituting equation (2.1) and integrating over all directions of **r** we get:

$$W = -4\pi G \int_0^\infty drr\rho(r)M(r) \tag{2.7}$$

The potential energy tensor of a spherical body is **diagonal** i.e it is isotropic, and has the form:

$$W_{jk} = \frac{1}{3}W\delta_{jk} \tag{2.8}$$

Once we have the general results for the potential of spherical distributions we can move on to study special cases, let's study potential-density pairs that would best fit for Globular Clusters.

The simplest model is the **homogeneous sphere** of radius a, characterized by the gravitational radius $r_g \equiv GM^2/|W|$, with $r_g = \frac{5}{3}a$, for which the gravitational potential is:

$$\Phi(r) = \begin{cases} -2\pi G\rho\left(a^2 - \frac{1}{3}r^2\right) & (r < a) \\ -\frac{4\pi G\rho a^3}{3r} & (r > a) \end{cases} \tag{2.9}$$

For spherical systems, the density is roughly constant near the center, and falls to zero at large radii. A potential of a system of this type would be proportional to $r^2 + constant$ at small radii and to r^{-1} at large radii. The **Plummer Model** is a simple potential with these properties and it it of the form:

$$\Phi = -\frac{GM}{\sqrt{r^2 + b^2}} \tag{2.10}$$

What characterises this model to a simple homogeneous sphere model is the linear scale that generates the potential, which is called the **Plummer scale length** b while M

represents the total mass of the system. From this potential, using spherical coordinates we can calculate ∇^2:

$$\nabla^2\Phi = \frac{1}{r^2}\frac{d}{dr}\left(r^2\frac{d\Phi}{dr}\right) = \frac{3GMb^2}{(r^2+b^2)^{5/2}} \tag{2.11}$$

And from $\nabla^2\Phi = 4\pi G\rho$ (**Poisson's equation**) the corresponding density to the potential:

$$\rho(r) = \frac{3M}{4\pi b^3}\left(1+\frac{r^2}{b^2}\right)^{-5/2} \tag{2.12}$$

And finally the potential energy of a Plummer model is:

$$W = -\frac{3\pi GM^2}{32b} \tag{2.13}$$

In 1911 Plummer used this potential-density pair to fit observations of Globular Clusters since it gets rid if the indetermination that would arise if we didn't include the Plummer scale length.

Another useful model is given by the **Isochrone Potential**, that gives analytic orbits to all the stars orbiting the system (For a Plummer potential the position of a star orbiting the system cannot be given in terms of elementary functions). This model is of the form:

$$\Phi(r) = -\frac{GM}{b+\sqrt{b^2+r^2}} \tag{2.14}$$

By Poisson's equation the density associated with the isochrone potential is:

$$\rho(r) = \frac{1}{4\pi G}\frac{1}{r^2}\frac{d}{dr}\left(r^2\frac{d\Phi}{dr}\right) = M\left[\frac{3\,(b+a)\,a^2 - r^2(b^2+3a)}{4\pi(b+a)^3a^3}\right] \tag{2.15}$$

So that in the extreme cases the isochrone potential yields:

$$\rho(r) = \begin{cases} \frac{3M}{16\pi b^3} & (r=0) \\ \frac{bM}{2\pi r^4} & (r \gg b) \end{cases} \tag{2.16}$$

As a very useful approximation, we can work with **Two-power density models**. First, we note that the luminosity density of many elliptical galaxies can be approximated as a power law in radius at both the largest and smallest observable radii, with a smooth transition between these power laws at intermediate radii. Some numerical simulations of the clustering of dark matter particles suggest that the mass density within a dark halo has a similar structure. This is the reason for which much attention has been given to models with a density of the form:

$$\rho(r) = \frac{\rho_0}{(r/a)^{\alpha}\,(1 + r/a)^{\beta-\alpha}} \tag{2.17}$$

Dark matter halos are often modelled by the above equation with $\beta \simeq 3$ and α in the range $(1, 1.5)$. Dehnen models are the solutions for $\beta = 4$ that have simple analytic properties. But we may discuss some specific results summarized in the following table:

Model	α	β
Hernquist (1990)	1	4
Jaffe (1983)	2	4
NFW (1995)	1	3

TABLE 2.2: Two-power densitiy potentials given by the different values of α and β

Navarro, Frenk, & White (1996) showed that the values taken by the free parameters α and β for the halos that formed in their simulations were strongly correlated, so the halos were essentially members of a one-parameter family.

According to equation (2.17) the mass inside the radius r is:

$$M(r) = 4\pi\rho_0 a^3 \int_0^{r/a} ds \frac{s^{2-\alpha}}{(1+s)^{\beta-\alpha}} \tag{2.18}$$

For the important cases we discuss, the mass is

$$M(r) = 4\pi\rho_0 a^3 \times \begin{cases} \frac{r/a}{1+r/a} & \text{for a Jaffe model} \\ \frac{(r/a)^2}{2(1+r/a)^2} & \text{for a Hernquist model} \\ ln(1+r/a) - \frac{r/a}{1+r/a} & \text{for a NFW model} \end{cases} \tag{2.19}$$

We can directly integrate the mass to get the potential for the three discussed models:

$$\Phi(r) = -4\pi G\rho_0 a^2 \times \begin{cases} ln(1+r/a) & \text{for a Jaffe model} \\ \frac{1}{2(1+r/a)} & \text{for a Hernquist model} \\ \frac{ln(1+r/a)}{r/a} & \text{for a NFW model} \end{cases} \tag{2.20}$$

From the above equations, and taking into account the potential energy for each model, it can be proved that the Jaffe and Hernquist models have gravitational radii $r_r = 2a$ and $6a$ respectively, while for the NFW model r_g is undefined. The circular speed, given by these potentials for each model is shown in the following figure:

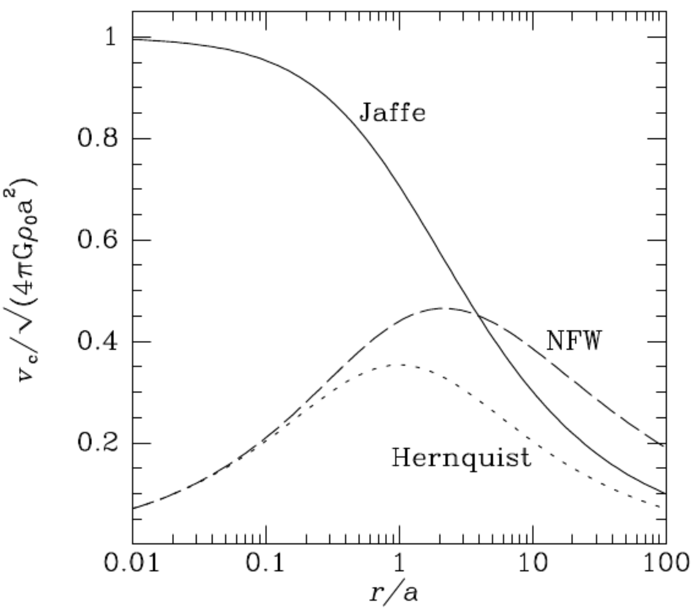

FIGURE 2.9: Circular speed vs radius for the models of Jaffe, Hernquist and NFW, taken from Binney & Tremaine, Galactic Dynamics 2nd edition.

The next step in the analysis of the dynamics and stability of Globular Clusters is to understand the physics of spherical distribution of systems and how the solutions for their dynamics can be easily reached. As we shall see, a good consideration for the simplification of the mathematical treatment of Globular Clusters (with good physical reasons) is that these systems are not collisional.

2.2.2 Collisionless Systems

The problem of modelling the structure and dynamics of Globular Clusters is not trivial whatsoever. Several assumptions and physical approaches need to be made to simplify the problem and reach results that fit the observational data. One of the main assumptions is that the stellar systems that we will study are **collisionless**. This assumption not only reduces the problem of determining the functional form of the position and velocities of the stars but also has strong physical reasons that must be mentioned.

In the context of stellar systems, collision refers to any interaction between individual particles, such as direct encounters, gravitational assistance, sudden disruption of the orbit, or any interaction that changes the stars orbit in a significant way. That the system is collisionless means that it is a system in which the interaction cross-section between particles (stars in this case) is so low that collisions between particles have no significant effect on the system so that the dominant component of the dynamics is the potential well produced by the system as a whole.

One of the other approximations we make is that the orbits of stars in the system can be determined by assuming that the mass of the Globular Cluster is distributed smoothly in space, rather than concentrated in certain positions as point masses. The true orbits deviate significantly from this approximated model, but in systems with more than a few thousand stars like a globular cluster (that can easily reach hundreds of thousands or millions of stars), the deviation is small and the potential and mass distribution can be approximate as continuous functions.

As a star moves through a stellar system, it will feel the gravitational force due to all other stars. We want to determine if the motion of the stars is mainly determined by the average gravitational force of all other stars combined, or if it is mostly sensitive to the force due to near stars, in order to do this we must refer to some parameters of time that we properly define like **relaxation** and **crossing** time.

Relaxation usually means the return of a perturbed system into equilibrium. In the clusters, stellar encounters eventually lead to dynamical relaxation, until we say that the system is in a thermal equilibrium.

The crossing time refers to the typical time that would take to a star to cross the whole system, in terms of the size of the system r and the velocity v of the stars, this time is:

$$t_{cross} = \frac{r}{v} \tag{2.21}$$

The relaxation time in terms of the crossing time and the number of stars N is:

$$t_{relax} = \frac{N}{8ln(N)} t_{cr} \tag{2.22}$$

As these quantities parametrize the interactions between stars, their values really give us a strong idea on how the dynamics can be modelled, as it was mentioned before, for a typical Globular Cluster, the evolution time t_{evo} is usually much larger than the relaxing time which is much larger than the crossing time, so the effects of the interaction between stars is minimal and we can use the approximation that the system is collisionless.

$$t_{cross} \ll t_{relax} \ll t_{evo} \tag{2.23}$$

2.2.3 Dynamics

Using the approximations we just mentioned, the dynamics of stars in Globular Systems can be solved assuming that the those stars are moving under a smooth potential $\phi(x, y, z, t)$ and that at any time t a full description of the state of these systems is given by specifying a function of the number of stars with their position and velocities $f(x, y, z, v_x, v_y, v_z, t)$ or $f(\vec{\mathbf{x}}, \vec{\mathbf{v}}, t)$ which is called the distribution function of phase space density because it is given in the phase space. This function is the number of stars in volume $d\vec{x}$ with velocities in range $d\vec{v}$ (centered on $\vec{x}, \vec{v}$).

This flow of points (or stars) of f is incompressible in the phase space (the density remains conserved along a flow-line) so that

$$\frac{df}{dt} = 0 \tag{2.24}$$

To infer properly the equation above and understand the time evolution, we define a coordinate $\vec{w}$ for the stars in phase space:

$$\vec{w} \equiv (\vec{x}, \vec{v}) \equiv (w_1, w_2, ...w_6) \tag{2.25}$$

The flow of the star is given by

$$\dot{\vec{w}} = (\dot{\vec{x}}, \dot{\vec{v}}) = (\vec{v}, -\vec{\nabla}\Phi) \tag{2.26}$$

The flow $\dot{\vec{v}}$ conserves stars so we have the continuity equation:

$$\frac{\partial f}{\partial t} + \sum_{\alpha=1}^{6} \frac{\partial (f \dot{w}_\alpha)}{\partial w_\alpha} = 0 \tag{2.27}$$

Using the chain rule for w our continuity equation explicitily in terms of the position and velicities is:

$$\frac{\partial f}{\partial t} + \sum_{i=1}^{3} \frac{\partial f}{\partial x_i} \dot{x}_i + \sum_{i=1}^{3} \frac{\partial f}{\partial v_i} \dot{v}_i = 0 \tag{2.28}$$

It is more useful to use the derivative of the velocity in terms of the potential with the relation $\dot{v_i} = -\partial\phi/\partial x_i$ as:

$$\frac{\partial f}{\partial t} + \sum_{i=1}^{3} \frac{\partial f}{\partial x_i} v_i - \sum_{i=1}^{3} \frac{\partial f}{\partial v_i} \frac{\partial \phi}{\partial x_i} = 0 \tag{2.29}$$

or

$$\frac{\partial f}{\partial t} + \nabla f \cdot \vec{v} - \frac{\partial f}{\partial \vec{v}} \cdot \nabla \phi = 0 \tag{2.30}$$

These equations are the Collisionless Boltzmann Equations (CEB) and they are sufficient to calculate the evolution of any distribution function f with time. As the CBE is a very complicated equation of 7 variables, its solution is a challenging task and some assumptions and creative methods have been developed for its solutions, one of them refers to the moments of the distribution function and the other is based on the Jeans theorem.

The moments approximation consists of considering that if the dependence of the phase space density upon velocity is relatively smooth and free of singularities, one can collapse the 6-dimensional phase space density into a set of functions of 3-dimensional position by taking moments of the velocities. First, let's note that the moment of order j of the distribution f is

$$\overline{x^j} = \frac{\int x^j f dx}{\int f dx} \tag{2.31}$$

We can define functions for the characterization of the distribution function on terms of one of its variables:

$$\nu(\vec{\mathbf{x}}) \equiv \int f(\vec{\mathbf{x}}, \vec{\mathbf{v}}) d^3 v \qquad or \qquad \xi(\vec{\mathbf{x}}) \equiv \int f(\vec{\mathbf{x}}, \vec{\mathbf{v}}) d^3 x \tag{2.32}$$

So that the zeroth moment of the velocity is just the number density $\nu(\vec{\mathbf{x}})$ and for each of three velocity components the first moment gives a mean velocity:

$$\bar{v}_i(\vec{\mathbf{x}}) \equiv \frac{1}{\nu(\vec{\mathbf{x}})} \int v_i f(\vec{\mathbf{x}}, \vec{\mathbf{v}}) d^3 \vec{v} \tag{2.33}$$

Likewise, we can define higher order moments with combinations of powrs of the three velocity components. The second moments give a really important and useful quantity related to the **velocity dispersion tensor** σ_{ij}^2

$$\overline{v_i v_j}(\vec{\mathbf{x}}) \equiv \frac{1}{\nu(\vec{\mathbf{x}})} \int v_i v_j f(\vec{\mathbf{x}}, \vec{\mathbf{v}}) d^3\vec{v} = \sigma_{ij}^2 + \bar{v}_i \bar{v}_j \tag{2.34}$$

The velocity dispersion tensor which will be fundamental in the mass modelling is thus defined as:

$$\sigma_{ij}^2 = \overline{v_i v_j} - \overline{v_i}\,\overline{v_j} \tag{2.35}$$

There is quite some observational support that ideally the velocity distribution functions are reasonably well described by the low order moments; a density and a set of low order moments may therefore give a reasonably complete description of a galaxy or a Globular Cluster.

Now to find the Jeans equations and show a different approach for the solution of the CBE we need to manipulate the results for the moments of the DF. By multiplying the CBE by powers of the velocity components, and integrating over velocity space we obtain a series of differential equations for the various velocity components on the zeroth moment, we have (using Einstein's notation of summation):

$$\int \frac{\partial f}{\partial t} d^3\vec{v} + \int v_i \frac{\partial f}{\partial x_i} d^3\vec{v} - \frac{\partial \Phi}{\partial x_i} \int \frac{\partial f}{\partial vi} d^3\vec{v} = 0 \tag{2.36}$$

Using the divergence theorem for the last term and replacing by the definitions of $\nu(x)$ and $\overline{v}_i \nu(x)$ we get:

$$\frac{\partial}{\partial t}\nu + \frac{\partial}{\partial x_i}(\nu \overline{v}_i) = 0 \tag{2.37}$$

Which looks just like a standard 3-D continuity equation. Now, we do the same procedure for the first moment, (again taking the spatial and temporal derivatives outside the velocity integrals) and integrating by pats and expressing the results in terms of our average velocities:

$$\frac{\partial}{\partial t}(\nu \overline{v}_j) + \frac{\partial}{\partial x_i}(\nu \overline{v_i v_j}) + \frac{\partial \Phi}{\partial x_i} \int f \frac{\partial v_j}{\partial v_i} d^3\vec{v} = 0 \tag{2.38}$$

The last term on the left hand side becomes $\nu\delta_{ij}$ in an orthogonal coordinate system. So applying the product rule and our continuity equation to the first term we get

$$\nu\frac{\partial\overline{v}_j}{\partial t} - \overline{v}_j\frac{\partial}{\partial x_i}(\nu\overline{v}_j) + \frac{\partial}{\partial x_i}[\nu(\sigma_{ij}^2 + \overline{v}_i\overline{v}_j)] = -\nu\overline{v}_i\frac{\partial\Phi}{\partial x_j} \tag{2.39}$$

Where we used the relation between the second moments and the velocity dispersion, finally differentiating the second term on the left hand side, part of the result cancels part of the third term and we arrive to the **Jeans' equations** for a collisionless fluid

$$\begin{gathered}\nu\frac{\partial\overline{v}_j}{\partial t} + \overline{v}_i\nu\frac{\partial\overline{v}_j}{\partial x_i} = -\nu\frac{\Phi}{\partial x_j} - \frac{\partial}{\partial x_i}(\nu\sigma_{ij}^2) \qquad (j = 1, 2, 3) \\ acceleration + viscosity = gravity + pressure\end{gathered} \tag{2.40}$$

One important use of the Jeans' equations is to calculate the number density and potential self-consistently, assuming a given model for the velocity dispersion.

The Jeans theorem states that any steady state solution of the CBE depends on the phase-space coordinates (x, v) only through integrals of motion in a static potential, and any function of the integrals yields a steady state solution of the CBE. The value of this theorem is that it gives us a way of closing the loop for solving the Boltzmann equation.

Finally, it is important to introduce a useful parameter called the **Anisotropy parameter** β which gives us information about the preferred directions of the stars in the system, if there are any. In spherical coordinates the anisotropy parameter is

$$\beta = 1 - \frac{\left(\sigma_\theta^2 + \sigma_\phi^2\right)}{2\sigma_r^2} \tag{2.41}$$

If $\beta = 0$, then $\overline{v}_r^2 = \overline{v}_\phi^2 = \overline{v}_\theta^2$ and we have zero anisotropy (there are no preferred directions for the stars in the system and the velocity dispersion tensor is completely symmetric) as in the ideal case of a spherical system in equilibrium. On the other hand, when $\beta = 1$ we have that the system has total anisotropy.

2.3 Scenario and Observations

The first globular cluster discovered, but then taken for a nebula, was M22 in Sagittarius, which was probably discovered by Abraham Ihle in 1665. This discovery was followed by that of southern Omega Centauri (NGC 5139) by Edmond Halley on his 1677 journey to St. Helena. This "nebula" had been known but classified as star since ancient times. Next followed the discovery of M5 in Serpens Caput by Gottfried Kirch in 1702, and that of M13 in Hercules, again by Halley, in 1714. De Chseaux's list of (21) nebulae of 1746 contains, in addition, two new globular clusters, M71 and M4, while Jean-Dominique Maraldi discovered M15 and M2 in September of this year (1746). Guillaume Legentil possibly or probably discovered NGC 6712 in 1749. Nicholas Louis de Lacaille's catalog of (42) southern "nebula" of 1751-52 contains 8 globular clusters (among them 5 new ones), while Messier's catalog of 110 objects contains a total of 29 globulars, 20 of them new discoveries. Charles Messier was the first to resolve one globular cluster, M4, but still referred to the other 28 of these objects in his catalog as "round nebulae." Thus, in summer 1782, before William Herschel started his comprehensive deep sky survey with large telescopes, there were 34 globular clusters known. Herschel himself discovered 36 new globulars, bringing the number of known globulars to 70. He was the first to resolve virtually all of them into stars, and coined the term "globular cluster" in the discussion adjacent to his second catalog of 1000 deepsky objects (1789).

there is widesprea belief that globular clusters cannot contain large amounts of dark matter, because of the Virial Theorem. This theorem relates the velocity dispersion σ at the center of the cluster to the total mass M_t and to the half-mass radius r_h of the system. For a one component globular cluster, that relation may be expresed as:

$$\langle \sigma^2 \rangle \approx 0.4 \frac{GM_t}{r_h} \tag{2.42}$$

However, if a dark component is also present, in the form of low-mass objects for example, the virial theorem must be modified to:

$$\sum_i M_t(i) \langle \sigma^2 \rangle_i = E_p \tag{2.43}$$

where the index i refers to the different stellar species, and E_p is the potential energy of the cluster.

2.4 Simulations

Efforts are under way by several groups to produce more realistic simulations that properly include the effects of star formation, but the existing results suggest that the first star formation may occur in gas that has become highly condensed at the centers of the first dark-matter halos to form; even though such systems may not closely resemble most present-day galaxies, they may still be of interest as the possible birth sites of globular clusters, as will be discussed further below. The most realistic simulations of the formation of a spiral galaxy like our own have been made by Katz (1992) and Steinmetz & Muller (1994, 1995), who have simulated the evolution of a spherical galaxy-sized piece of a standard "cold dark matter" universe which is arbitrarily given the appropriate amount of angular momentum. The results show an initial chaotic stage during which mergers between clumps build up a dark halo and a stellar spheroid, followed by a period during which the remaining gas organizes itself into a disk. During the initial chaotic stage several small satellites are formed by the condensation of gas in peripheral dark-matter clumps, and these satellites may survive for a few orbits before being disrupted and merged into the forming galaxy. It is plausible that such small satellites could be the birth sites of globular clusters, as in the hypothesis of Searle (1977) and Searle & Zinn (1978) that the globular clusters in the outer halo of our Galaxy were formed in protogalactic fragments which survived for a time as independent star-forming systems before being merged to build up the halo

In several earlier reviews of globular cluster chronology, it was concluded that the globular clusters in our Galaxy are not all coeval and that age differences of several Gyr exist in at least a few well-studied cases (e.g., Larson 1990a, 1992b). This conclusion still appears to be valid, and it is supported by the most recent discussion of this subject by Chaboyer, Demarque, & Sarajedini (1996), which is based on new age estimates for 43 globular clusters

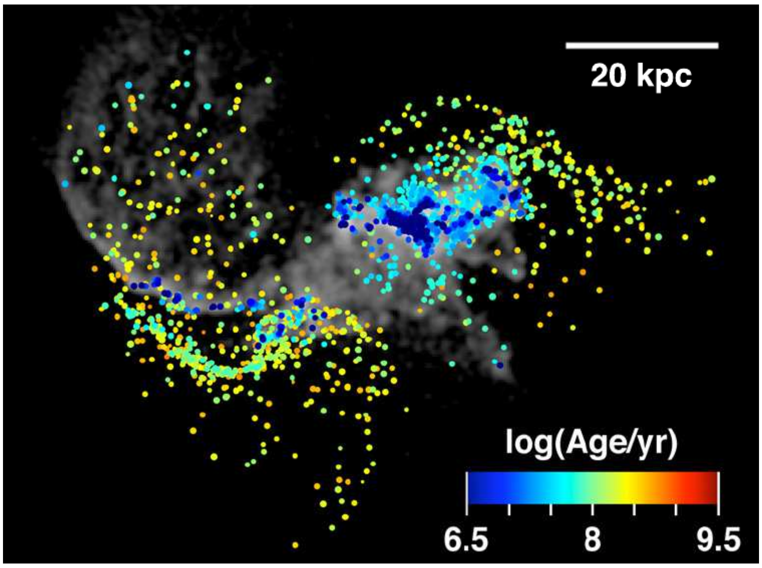

FIGURE 2.10: Snapshot of galaxy merger model 1m11 from Kruijssen et al. (2012b), which includes a sub-grid model for the formation and evolution of the stellar cluster population. SHown is a merger of two Milky Way-mass galaxies at the time of their first encounter. Coloured dots represent stellar clusters, clour-coded by their ages as indicated by the legend. The grey scale indicates the gas surface density. The snapshot shows how intermediate-age clusters are escaping into the halo, whereas those clusters that formed during the merger reside in the gas-rich, disruptive environment of the discs. This cluster migration process is also seen in observations of nearby galaxy mergers (Bastian et al. 2009).

Chapter 3

Observations and Analysis

In order to study this problem about the dynamics of Globular Clusters in our galaxy we need scientific data that allows us to build a model that fits our observations. Under supervision of proffesor Juan Carlos Muñoz Cuartas and with three other undergraduate students from the University of Antioquia a trip to the OPD (Pico dos Dias Observatory) was made to Brazil in May 2014, besides the observational experience of the students, the main purpose of the trip was to get important data for this project. We needed two sets of data corresponding to spectra and photometric images of the Globular Clusters

The spectroscopic data allows us to determine the velocity dispersion profile in the inner region of globular clusters while the photometric data allows us to study the surface brightness distribution for them. We can use all of this information to infer the properties of the globular clusters' mass distribution in order to build complete dynamical models and therefore infer the amount of dark matter present in the globular clusters (if there is any).

3.1 Observational Procedures

Our stay in OPD consisted of two days in the main dome for the spectroscopic data (using the Perkin-Elmer (P&E) telescope with a 1.6m mirror and the Cassegrain Spectrograph) and four days in a smaller dome for the photometric data in the IAG telescope with a 0.6m mirror. In the following photograph, the domes of the observatory that we used for our observations:

FIGURE 3.1: OPD observatory seen from the air, the big dome was used for the spectroscopic data and the small dome at the low right part of the photo for the photometric data.

3.1.1 Spectroscopic Data

The first two days (May 14th and 15th) we took the spectroscopic data in the telescope P&E with a diameter of 1.6m. The main instrument was the Cassegrain spectrograph with a CCD Ikon-L camera and Filters BVR. The software we used was the recently installed software TCSPD which is built in a LabView environment for Windows (2010). Here's a photo of the telescope from inside the dome:

FIGURE 3.2: Perkin-Elmer telescope in the main dome in OPD used for the spectroscopic observations

We made the observations of dome flats, bias frames, comparison lamp frames, calibration stars, some galaxies and certain globular clusters of the milky Way organized by the best observation times using Simbad and Stellarium for the estimations of the coordinates and times respectively. The objects we observed in OPD are organized in the following table

Object	α	δ	**05/14**	**05/15**	**05/16**	**05/18**	**05/19**
NGC5020	13:12:39.87	+12:35:59.0	✓	✗	✗	✗	✗
NGC5272	13:42:11.62	+28:22:38.2	✓	✓	✓	✗	✗
NGC4833	12:59:33.92	-70:52:35.4	✓	✗	✗	✗	✗
NGC4590	12:39:27.98	-26:44:38.6	✓	✓	✓	✗	✓
NGC5139	13:26:47.28	-47:28:46.1	✓	✓	✓	✓	✓
NGC5286	13:46:26.81	-51:22:27.3	✓	✓	✗	✗	✓
NGC6752	19:10:52.11	-59:59:04.4	✓	✗	✗	✗	
NGC6397	17:40:42.09	-53:40:27.6	✓	✓	✓	✗	✓
NGC6723	18:59:33.15	-36:37:56.1	✓	✓	✗	✓	✓
NGC7615	23:19:54.44	+08:23:57.9	✓	✗	✗	✗	✓
NGC6541	18:08:02.36	-43:42:53.6	✓	✓	✗	✓	✓
NGC2802	09:16:41.41	+18:57:48.8	✗	✓	✗	✗	✗
NGC5024	13:12:55.25	+18:10:05.4	✗	✓	✗	✗	✗
NGC6362	17:31:54.99	-67:02:54.0	✗	✓	✗	✗	✗
NGC6502	18:04:13.68	-65:24:35.7	✗	✓	✗	✗	✗
NGC7078	21:29:58.33	+12:10:01.2	✗	✓	✗	✓	✗
NGC7099	21:40:22.12	-23:10:47.5	✗	✓	✗	✗	✗
NGC6970	20:52:09.46	-48:46:39.8	✗	✗	✗	✗	✓
NGC6541	18:08:02.36	-43:42:53.6	✗	✗	✗	✗	✓
NGC6715	18:55:03.33	-30:28:47.5	✗	✗	✗	✗	✓
HR4963	13:09:56.99	-05:32:20.4	✓	✗	✗	✗	✗
HR4468	11:36:40.91	-09:48:08.1	✓	✓	✗	✗	✗
HR7950	20:47:40.55	-09:29:44.8	✗	✓	✗	✗	✗
HR4961	13:09:45.28	-10:19:45.6	✗	✗	✓	✗	✗
HR6308	16:59:57.71	-25:05:31.9	✗	✗	✗	✓	✓
HR7964	20:49:20.54	-18:02:09.1	✗	✗	✗	✓	✗
HR6386	17:12:13.62	-25:15:18.6	✗	✗	✗	✗	✓

TABLE 3.1: Observed objects in OPD observatory, the table contains the equatorial coordinates of the objects and the days each object was observed, the check mark indicates that the object was observed and the x mark indicates it was not observed. The details of the observations for each day are explained right ahead.

Now, our set up configuration for the spectrograph was the following:

On May 14th, a diffraction grating of 900 lines per mm, a CCD IkonL and the central wavelength for the observations of 8500 Angstroms (with possibility of rotation of the slit 90, +45 and -45).we used the slit of 2.52" and obtained data for the globular clusters: NGC5020, NGC5272, NGC4833, NGC4590, NGC5139, NGC5286, NGC6752, NGC6397, NGC6723, NGC6715 and NGC6541 using exposition times of 600 and 900 seconds. We also observed the calibration stars: HR4963 and HR4468 with 7 and 5 seconds. As it was the first day, we needed to be very careful in calibrating our instruments on order to have the objects in the right focus, we also made the rotation of the slit to use all the diffraction angles of the observations and our comparison lamps were of Ne-Ar.

On May 15th, we used the slit of 3.0", and used a central wavelength of 5500 Angstroms. This time we observed the following objects: NGC2802, NGC5024, NGC4590, NGC5139, NGC5286, NGC5272, NGC6362, NGC6397, NGC6723, NGC6502, NGC6541, NGC7078, NGC7099, the stars HR4468 and HR7950 and we also observed Mars for pedagogical reasons. We used pretty much the same exposition times than the day before, this time though, our comparison lamps were or He-Ar. All the data we took was in FITS format (Flexible Image Transfer System).

3.1.2 Photometric Data

The photometric data were acquired in the next four days (from May 16th to May 19th) in the 0.6m IAG telescope in OPD. We used the Johnson system for the different filters which were easily shifted with the given software in the control computers. Here a picture of the telescope from inside the dome:

FIGURE 3.3: IAG telescope used for the photometric data

On May 16th, we took all the calibration images, consisting of 20 bias frames with an exposition time of 0,00001 seconds; also 22, 11, 11, 20 and 10 flat frames for the B,I,R,U,V filters respectively, their exposition times differed, for U filter we took various frames of 60 and 30 seconds, for the B filter we took frames of 30 seconds each, 15s for I, 60s for R and 3s for V. We took our "focus" images to calibrate the instrument, and also various skyflats for all the filters. We targeted the following globular clusters and calibration stars in different filters: NGC5272, HR4961, NGC4590, NGC5139 AND NGC6397. The exposition time for the clusters was of 600 seconds and 2 and 4 seconds for the calibration star.

May 17th was a terrible night for observations because the sky was too cloudy and the only useful data we could get were dome flats for the filters I,R and V that we could use instead of the bad dome flats of the first day. The reduction using the flats of another day are decent but this is not the ideal situation since mechanical movements of the instrument might slightly change its configuration and therefore it probably ends up with a reduction that is not the ideal one for science purposes.

On May 18th we were more organized since we were getting familiar with the observations and therefore the data we got had little trouble in the upcoming analysis, even though the sky was clody at the end of the night. The science objects we observed were NGC5139, HR6308, NGC6723, NGC6541, NGC7078, HR7964 that were observed in the different filters. We got 20 bias frames, 14 dome flats in the vaious filters, but no skyflats.

On May 19th we observed the Clusters NGC5139, NGC4590, NGC6723, NGC6715, NGC6541, NGC6970, NGC5286, NGC6397, NGC6541 and NGC6715, the calibration stars HR6386 and HR6308, 20 bias frames and flats for each filter.

3.2 First step for Anaysis

Our first goal in starting the analysis of all the relevant data was to organize all the images in order to reduce the time required to make the reductions. For every day the calibrations images, trash, calibration stars and objects were separated and they were given their correct names as they were in the headers and compared with the information sheets we filled at the time we were doing the observations. With the use of an account on the galaxy.udea.edu.co cluster, for proper and quicker analysis and safety of the data, all the files were correctly organized.

The next step was the reduction of all the images with the calibration files for each day, I started the photometric data to acquire certain skills in the use of IRAF because the reduction of the spectroscopic data was to be a little more complex and needed a deeper understanding of IRAF packages.

I started with the cluster NGC-5139 (ω Centauri) because we got lots of data for that cluster in OPD and also because ω Centauri is a well known globular cluster since it is the largest in our galaxy and we can get a lot of information from the web.

After the photometry of that cluster, the most relevant part of the reduction was to be made. The reduction and analysis of the spectroscopic data (May 14th and 15th), the methods for these reductions are quite special and are the most relevant part of the analysis because that is our most valuable information. The reduction was to be made very carefully because a good spectroscopic analysis depends upon a good reduction of the data. Just as with the photometric data, the first procedures were made for the Cluster NGC5139 to understand and master the techniques of the reduction and extractions.

3.3 Photometry

The photometry was made by the two traditional methods, PSF photometry and Aperture Photometry; even though the magnitudes calculated using both methods are quite different, the calibration constant between the two methods gave a good relation between them and made us trust the photometry results.

But first, the reduction of the data had to be done. The first step is to characterize the calibration images in order to see if there are any errors associated with the instrument or the way that the observations were made. By doing this we found that most of the flat-field images had brightness gradients in the corners and this was a problem we needed to correct because the increased value on the counts in these corners would affect the normalization of the super-flat that we would use to reduce the science data. Another systematic error that we found in all of our calibration and science frames was the presence of a strange water-looking figure at the top left corner of them, although it can be removed with the correct reduction, it obviously affected the CCD sensitivity by the time of the observations. Also, some filters showed a higher sensitivity to this systematic errors but at the end, the photometry could be made in the best data so that the dirty images don't affect our results.

In order to see how the data would be affected by the systematic errors we just mentioned, we produced a composite image using three images with the filters U,V and R and we did the same with the flats in those filters, the results are shown in the following figure:

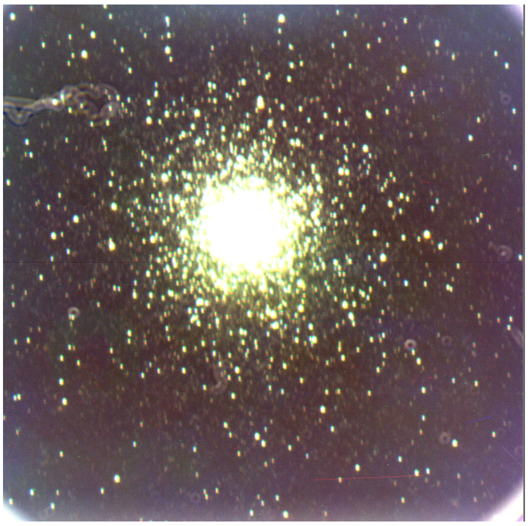

FIGURE 3.4: Composite image of NGC5139 without being previously reduced

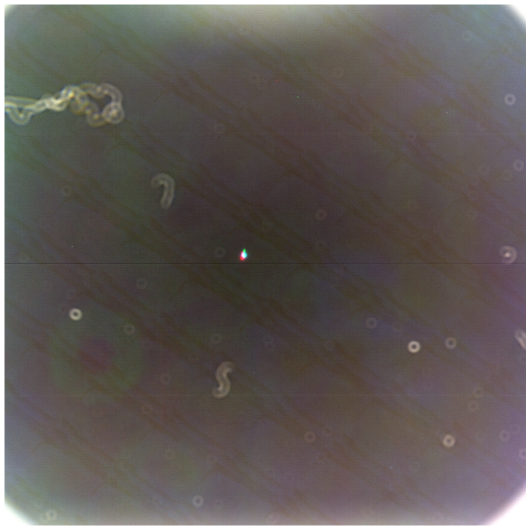

FIGURE 3.5: Composite image of the flats showing the noise that needs to be extracted

What we can infer from these images is that the flat fields and the bias frames contain the same noise that the science data thus giving us a good result in the reduction.

Once all the characterization is made we can reduce our important data using IRAF following the conventional steps consisting of:

- Building a Superbias: *Zerocombine* allows us to create the superbias using the median.

- Substracting the Superbias to every flat and science data: We substract the Superbias to every flat frame with no distiction on the filter, this is easily made using the task *imarith*, we also substract them from the original science images.

- Building Superflats: It is necessary to create a Superflat frame for each filter because the response of the CCD and will be different for different wavelengths, we use *imcombine* to do this and this time we use the mode for better results.

- Divide the Superflats by the median: In order to normalize the flatfields we find the mode of each frame with *imstatistics* and then divide them by that value

FIGURE 3.6: Example of one of the Normalized Superflats for the I filter

- Reduce the science data: Finally, we divide the original images of the clusters and stars (with the bias substractet) by the normalized Superflat to get the reduced images. This can easliy be made using the task *imarith*.

3.3.1 Aperture Photometry

Now that the reduction has been made and the corrections pixel by pixel have been applied, we can proceed to do the photometry using the simplest technique, known as Aperture Photometry which consists of adding up the pixel counts within a circle centered on each star of the cluster and subtracting the quotient of the per-pixel average value of nearby sky count divided by the number of pixels within the aperture. This will result in the raw flux value of the target object. This Aperture Photometry was done using the task *Phot*:

For stars in the NGC5139 cluster, one must choose a very small aperture of the sky because the surrounding stars contribute to the flux that needs to be extracted and they are very close to each other, as we can see in the following figure:

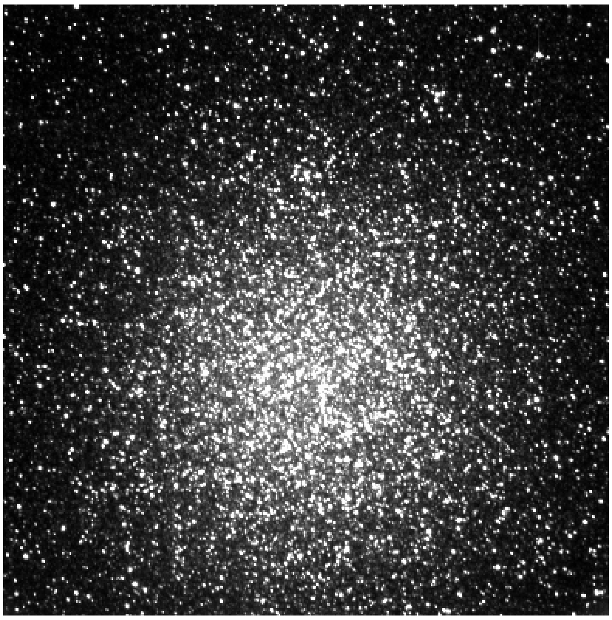

FIGURE 3.7: One of our observations of NGC5139 in the V filter with an exposition time of 480 seconds

with the task *imexamine* I find a value for the FWHM of 6.4 which I will use to set the size of the apertures to do the photometry. For the size of the aperture containing each star I chose an aperture size of four times the FWHM of the point spread function associated to the stars because it is the one that best fits the photometry and minimizes the error (calculated for some stars pressing "a" with the *imexamine* task) and for the width of the aperture I chose I value of 2.5 times the FWHM.

Another important value to take into account before editing the parameters in *phot* is the medium value of the background on the sky, in the case of this cluster, I do an average on many different places in the background of the image and find a value of sigma for the image that is equal to 53.45.

Now the photometry is done by changing some of the parameters including the readnoise and the gain. In the *fitskyparts* task inside phot I set the inner radius called annulus to be 25.6 (4FWHM) and the intermediate width called dannulus of 16 (2.5FWHM). Finally, before running the task I make sure I do the photometry using various apertures because I want to see which one minimizes the errors. I set apertures to be 1FWHM, 1.5FWHM, 2FWHM, 2.5FWHM, 3FWHM, 3.5FWHM and finally run the task. The results of the magnitude found for one of the star as a function of the size of the aperture is displayed below:

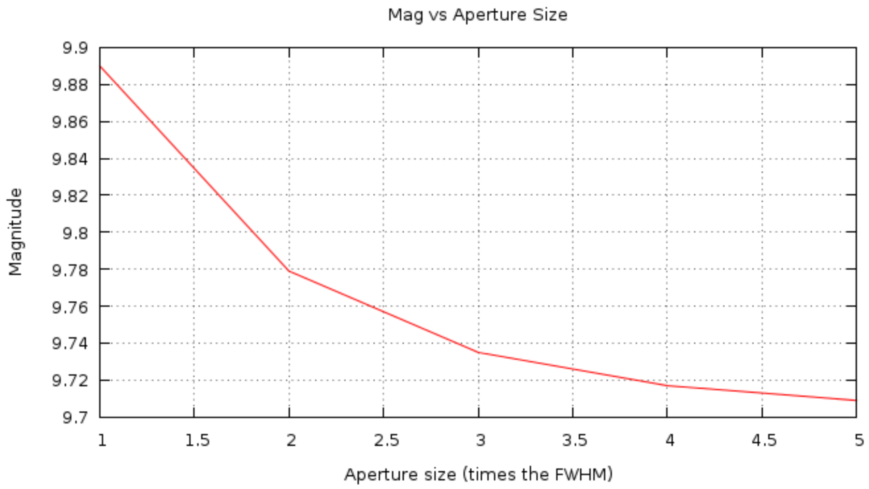

FIGURE 3.8: The magnitude decreases for bigger appertures

As we can see in the figure above, the magnitude of the chosen star in the cluster decreases for bigger appertures but so does the error because the space around the star is crowded of more stars and noice coming from the stars in the background so we infer that for crowded areas like this one the best choice is a small aperture. Although the results may not be as convincing, the use of another technique of photometry allows us to compare the results and see if the choice of a small aperture is a good way to fix or avoid the problem of the big noice of the background. For this purpose we use the technique of Point Spread Function (PSF) Photometry.

3.3.2 PSF Photometry

There exist many ways to count photons for an image taken with a CCD camera, but all of these ways obey the same principle of energy distribution in luminous objects. The point spread function for each of these objects is an assigned measure from the probabilistic distributions that approach quite well to the count of photons that one wants to do in the photometric analysis of astronomical images. The PSF photometry technique makes the most of the PSF of the objects using certain packages and tasks in a slightly different way than aperture photometry.

When doing photometry in a very crowded field, such as a globular cluster (NGC5139 in this case), where the profiles of stars overlap significantly, one must use de-blending techniques, such as point spread function (PSF) fitting, to determine the individual flux values of the overlapping sources.

This time, I made PSF photometry to some of the stars in the same cluster I started with (NGC5139), I chose bright ones that were relatively isolated to surrounding stars in order to make the estimations more accurate. First I use the same value of the PSF of some of those stars that I found doing the aperture photometry (6.4), this time the value of the sky is going to be higher because this value is going to determine the ammount of stars that the task *daofind* will select to do the photometry and I'm only interested in the brighter ones, a value of 2000 would filter out many of the fainter stars and the background. This values is using the standard deviation and making an average over many values found by the command "m" in the interactive mode of *imexamine*.

After setting all the parameters of *phot*, *daopars* and *findpars*, I run *daofind* which will find the stars that match the criteria I mentioned above and will create a text file with the coordinates of those stars and will give to each star an ID.

The task *tvmark* allows me to highlight the stars of the cluster in the display mode using the text file with the coordinates, and *txdump* allows me to put explicitly the coordinates of those stars in a text file that I use for the aperture photometry to make the first guess of the PSF of the stars.

The best way to correctly select the stars that will be used for the modelling of the PSF is by using the task *pstselect* that will select the stars that are well isolated using statistical techniques.

Once the stars are selected, the next step is to use the task *psf* which matches the point spread functions of the input images, by running this task, one can visualize how the PSF is modelled for each star and accept or decline the results to be stored, the interactive mode allows us to take the decision by analysing the modelling like the one we can see in the following image of the xterm:

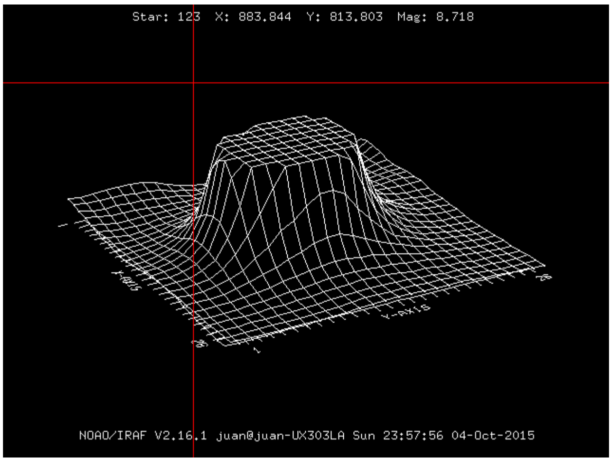

FIGURE 3.9: PSF modelling, the interactive mode allows us to accept of decline the result by pressing "a" or "d", in this case the PSF is not a soft curve with a Gaussian behaviour so it can probably be discarded

After running *psf*, there will be created an image that contains the residuals of the psf modelling which can be seen like this:

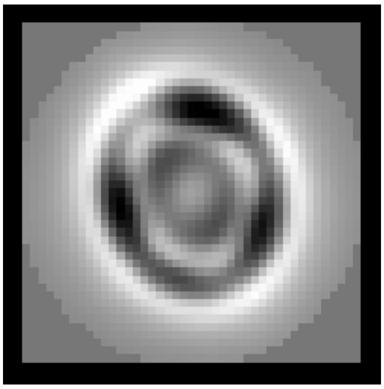

FIGURE 3.10: PSF residuals

With the task *seepsf* another image will be created but this time it will actually look like a star:

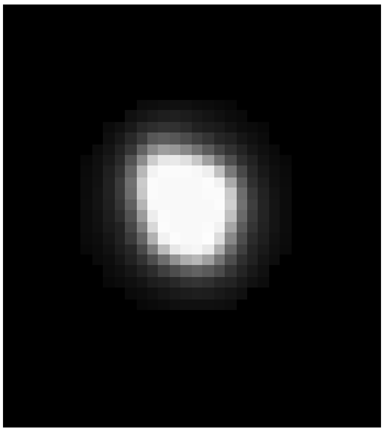

FIGURE 3.11: Seepsf converts a sampled PSF lookup table to a PSF image which can be visualized

Finally, after the modelling of the PSF was made, the task *allstar* does the photometry of the cluster using the results we just stored in the current directory. The results of the PSF photometry gave us magnitudes smaller for those stars than the results given by the aperture photometry but there is a constant difference for all the stars which we can assume to be a calibration constant between the two methods.

3.4 Spectroscopy

This is the most important part of the observational part of this project since the spectroscopic data has the most valuable information about the Globular Clusters and because our data were obtained in the largest and best telescope in OPD. Also, spectra of this kind is not easy to find in the scientific databases so we have important data to work with. The first spectroscopic procedures were also made for the ω Centauri cluster since we need to master the reduction and extraction techniques first in order to be able to start the scientific work about the mass modelling of the clusters.

3.4.1 Spectroscopic Reduction

The spectroscopic reduction is made by following some steps taking into account that we did not take any Skyflats so we need to create a response function using our dome flats. The steps are:

- First we make a Superbias combining all the bias frames and then we subtract it from all the lamp, targets and flat field frames.

- It was important to analyse the flats to see which ones are saturated, we consider that values over 65,000 counts (using implot) show saturated data. The ones that we could trust for May 14th were ten images called flats_0012 to flats_0021.

- The pre-superflat is made using the median given the number of images.

- We need to make a trimming in all images because there are some regions in the images that show unexpected luminosity, this is probably due to border errors in the camera or the obturator time of relaxation. The zones we decided to cut were:

[0-100] and [575 to the end]

- A critical step is the creation of a response function, this is made by collapsing the pre-superflat to one column using *blkavg*. The useful image for the creation of the Superflat is done by combining this column with *blkrep*. This gives us an image that's uniformly distributed in the dispersion axis with the following IRAF commands.

blkavg MasterFlat.fits[1:475,*] AvgFlatCols 475 1

blkrep AvgFlatCols AvgFlatColsMaster 475 1

- The pre-superflat is now divided by the response function we created (AvgFlatCols-Master) and this gives us the Superflat that we will use to reduce our data.

- Finally, the task we use to remove the cosmic rays is *lacos*, and it gives very accurate results, as it shows the "mask" image with the removed cosmic rays.

The vertical axis of the spectra is the dispersion axis and the horizontal axis is the spatial separation between stars. To visualize the reductions we have the following figures taken from the dirty and reduced NGC5139 spectrum (Day of observation May 14th):

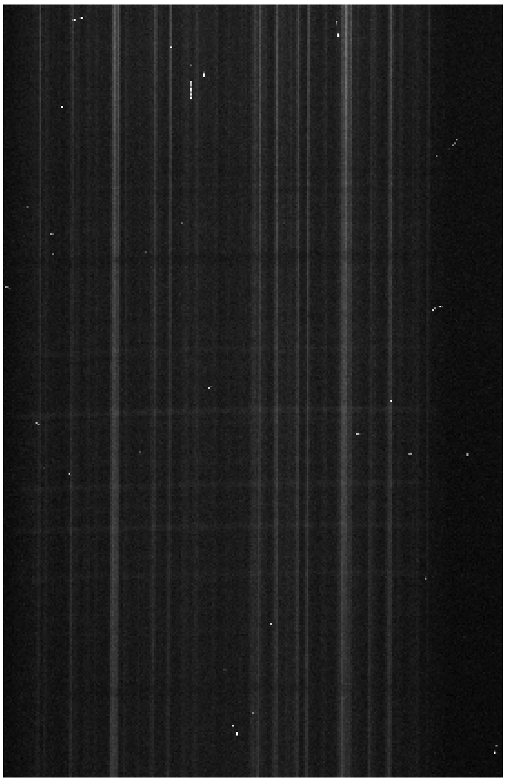

FIGURE 3.12: The dirty cluster spectrum has a small signal to noise ratio, besides border effects (such as a big gradient) that need to be trimmed and cosmic rays.

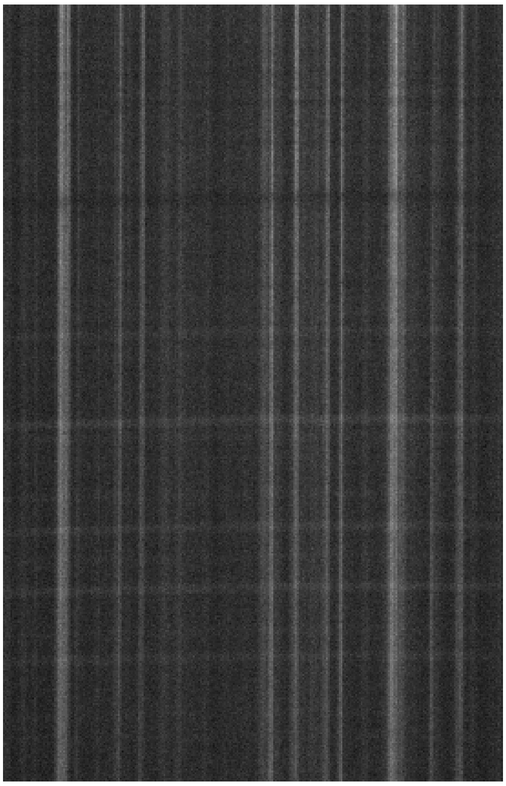

FIGURE 3.13: The clean spectrum without the bad data at the borders that needed to be trimmed, with a higher signal to noise ratio and the cosmic rays removed,

The images above are just a fraction of the whole image which is actually longer in the vertical direction, we chow only a fraction for visual purposes. As we did not take skyflats, some telluric lines are visible even in the reduced spectrum but this can be solved doing a correct calibration and carefully examining the extraction of the spectra of the stars.

3.4.2 Extraction

Once the reduction is ready, we can proceed with the extraction of the spectra of the calibration stars and also the spectra of the stars in the clusters, this procedure is made with the task *apall*. First, I did the extraction of the two calibration stars for each night of observation. For May 14th our calibration stars were HR-4963 and HR-4468 and for May 15th our calibration stars were HR-4468 and HR-7950.

Taking special care of correctly choosing the background, and with the following parameter configuration:

b_number: 100

background: fit

weight: variance

saturate: 65215

rdnoise: 6

gain: 1

Interactively, one must choose very precisely the background regions to extract the spectrum and do the fitting routines with different orders until the best results are reached, the areas of the background are changed using the commands "b" (for setting the background mode) and "s" (for setting the range). A good choice for the background in the case of the calibration star is relatively easy but in the case of the extraction of the stars in the clusters one must take into account the high noise introduced by the other stars and the background so for every star one must zoom into the window using "w" and "a" between the boundaries of the range to be zoomed.

If a good choice of the background and the dispersion axis is well fit, the task runs straightforward to get the spectrum of the star. In the case of the calibration lamps, the procedure is quite similar because the extraction of their spectrum is done with *apsum*, which is very similar to *apall*.

For the calibration star HR4468, the extracted spectrum looks like this:

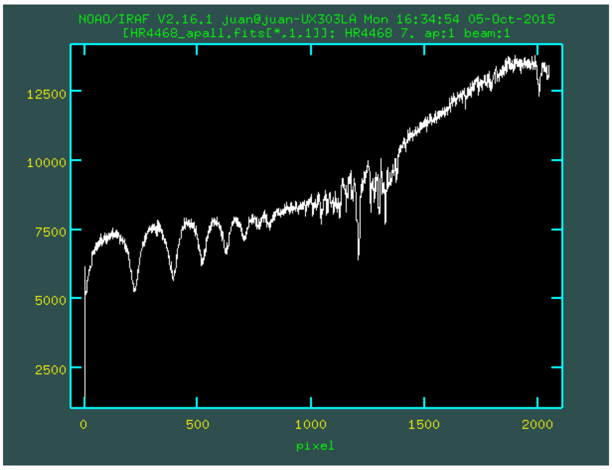

FIGURE 3.14: Extracted spectrum of HR4468, note that the dispersion axis is still in terms of pixels instead of Angstroms, this is fixed by doing the wavelength calibration, also the direction will be shifted because the strong sodium absorption lines are in the left end of the spectrum and they should be in the right end

3.4.3 Wavelength Calibration

Once the spectrum is extracted, the following step is to calibrate it in wavelength in order to make it useful for scientific analysis.The wavelength calibration is made many tasks of IRAF like *Identify*, *Refspec* and *Dispcor*. First, with *identify* I use the interactive window in IRAF to select some prominent lines in the spectrum of the calibration lamps and assign them their correct wavelength using the theoretic spectrum of the lamp. In this case our calibration lamps were Ne-Ar (for May 14th) and He-Ar (for May 15th) and OPD observatory provided us the theoretic distribution of emission lines of them. As we can see below:

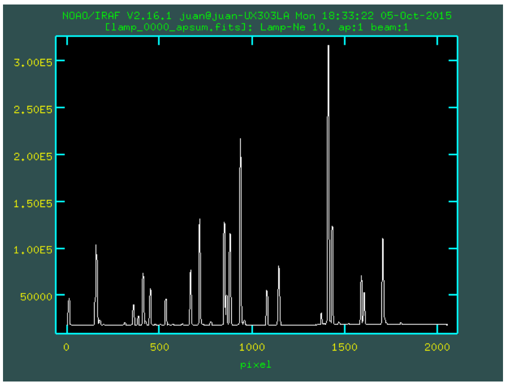

FIGURE 3.15: Emission lines of the Ne-Ar calibration lamp that need to be wavelength calibrated ,the horizontal axis is in pixels and needs to be calibrated to units of wavelength

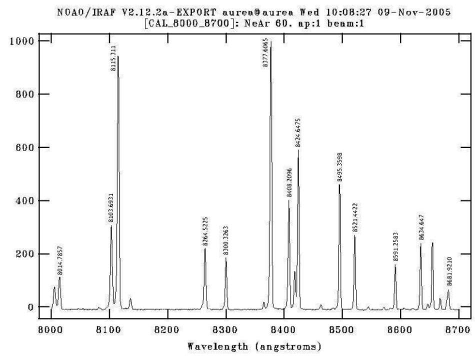

FIGURE 3.16: The theoretic emission lines of the Ne-Ar lamp provided by OPD that we use to make the wavelength calibration, note that the lines to be matched are going in the opposite direction

Running *identify* in the interactive mode and using "m" to select the larger lines and typing the wavelength, the task creates a file stored in a new folder "database" with the pixels with their corresponding values in units of Angstroms. After that, the targets (Calibration Stars and Globular Clusters) were to be calibrated with these files so it is necessary to edit their header to assign them the reference frames. It is enough to change the REFSPEC1 image header on each lamp file in order to set the wavelength calibration.

The task that actually does the calibration on wavelength for the science targets is *dispcor*, it is only necessary to run the task over all the targets with their own wavelength calibrated lamp to get the calibrated spectrum which is the useful and important file to make the analysis of the width of the lines and their redshift.

The wavelength calibrated spectrum of the star HR4468, after running *dispcor* is:

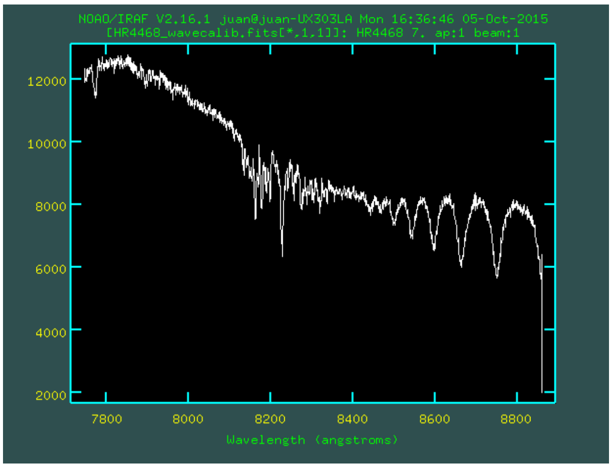

FIGURE 3.17: The spectrum has been wavelength calibrated as we can see in the horizontal axis which is in units of Angstroms. Note that the strong absorption lines are now in the right part of the spectrum, this is because in the process of making the wavelength calibration, the direction of the axis was changed.

3.4.4 Flux Calibration

This final part of the extraction and calibrations has the aim of calibrating the CCD chip response, spectrograph+telescope throughput and allow for atmospheric extinction. The result is a spectrum as observed from outside the atmosphere with an ideal uniformly sensitive detector+telescope+spectrograph. Basically, what the flux calibration does is, it takes from a tabular compilation the energy distribution of the standard star, it corrects this energy distribution for wavelength-dependent atmospheric extinction, it compares it to the energy distribution of the observed spectrum and derives from such a comparison the function that gives the response of our system for every wavelength.

The flux calibration takes place in three parts: Calibrating from the standard star, calculating the sensitivity function of the instrument, and finally, applying the calibration to the spectra. We will use the task *observatory* to determine observatory parameters, *standard* to flux calibrate each standard star, and *sensfunc* to finally determine the wavelength response and the solution will be applied to the spectra by the task *calibrate*.

In the first part, the calibration is made with one of the stars that are already included in IRAF, there are many stars so there's quite a good amount of options to choose. So the first task is the task *standard*. The observatory parameter is specified as LNA (Laboratório Nacional de Astrofísica) which is in IRAF's database.

The task standard

The task standard determines calibration pass-bands and writes them to a file called "std". The trick here is to specify the location of the the input extinction and flux calibration files. To do that, I edit the parameters of standard with the following routes:

Extinction file: onedstds$/ctioextindt.dat

Directory containing calibration data: onedstds$ctionewcal/

Starname in calibration list: l9239

Where I chose the Star l9239 because it has the spectral range that we use in our calibration Stars. And running the task interactively would be enough for this step.

The task sensfunc

The task *standard* just recorded response of each standard star so the next step is to put the results together and find a proper wavelength dependence of instrumental sensitivity and atmosphere transparency using the task *sensfunc*. It creates an image with a default name sens.0001. IRAF needs to have some general idea of atmospheric extinction before to start, so I set again extinct onedstds$ /ctioextinct.dat.

Now, running the task interactively and taking into account that the function used to fit the instrumental response will be usually of very high order. A good idea is to use spline3 fitting (:function spline3) with some 20 pieces, i.e. (:order 20). Finally "q" exists the *sensfunc* task and writes the sens.0001 image.

The task calibrate

The solution to each star to be calibrated is done with the task *calibrate*. Editing the parameters of calibrate to set the appropriate extinction table: extinct onedstds$ /ctioextinct.dat would be enough for this purpose. The task is run over all the wavelength calibrated spectra which had their airmass and other parameters appropriately set by the eso.set procedure. And finally it gives the flux-calibrated spectra ready for the relevant analysis concerning radial velocities.

After the flux calibration, I notice that the extremes of the spectra have irregularities given by the flux calibration procedures, but that can be cut because they don't have any relevant information.

For the star calibration I cut from 0 to 45 and from 1860 to the end, using imcopy:

imcopy flux_calib_star_fits[45:1860,*] cut_flux_calib_star.fits

The wavelength and flux calibrated spectrum of the star HR4468, now ready to be used for radial velocities determination looks like this:

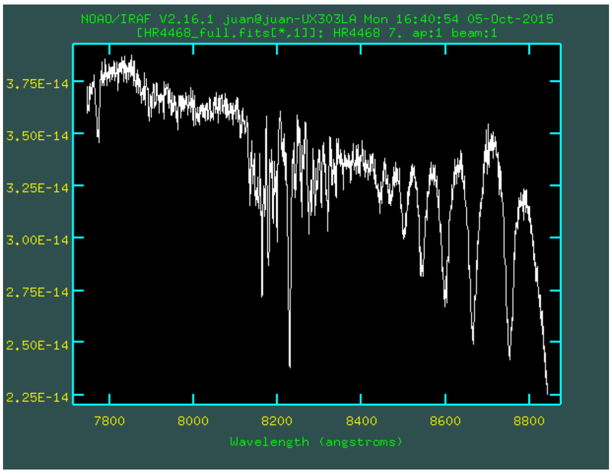

FIGURE 3.18: Flux calibrated spectrum of HR4468 calibration star

In order to normalize the spectrum, first I find the maximum value in the spectrum using minmax and then I divide the whole image by this value.

Something that can be very usefull is to have the data of the spectrum in a different format so that it's information can be well used and analyzed with simple programs like gnuplot, for this purpose, it is useful to create an Ascii table from the spectrum. For this purpose I need to first convert my image to a 1D image using the task *scopy* and setting format=onedspec (this is only neccesary if the specrtum was extracted in 2-D).

Now, with the image ready in 1-D, I use the task *wspectext* to create the Ascii table like this:

wspectext ready_flux_star.0001.fits normal_cut_flux_star_calib.txt

In principle, the same procedures halt for the star in the Globular Clusters, even though it must be made more carefully because the background noise and the crowded space surrounding them affects the spectra and it might change the values of the radial velocities, an example of a wavelength and flux calibrated spectrum of one of the stars in the NGC5139 cluster is:

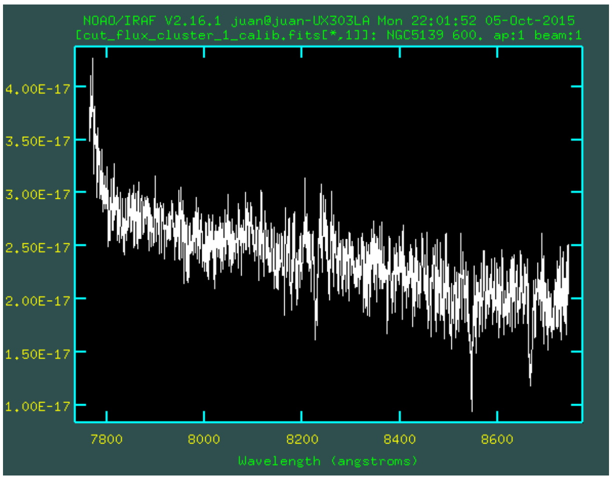

FIGURE 3.19: Spectrum of one of the most prominent stars in the NGC5139 cluster, after all the calibrations have been made

Although the noise is evidently higher than in the case of the spectrum of the calibration star, it is possible to see (even with the naked eye) two of the calcium strong absorption lines around 8543Å and 8663Å. After all of these procedures have been made to the important stars in the clusters and the calibration stars, the next step is to explore the best way to determine radial velocities with the use of some sophisticated tasks in IRAF such as *RVSAO*, as we discuss in the next section.

3.5 RVSAO and radial velocity determination

bcvcor:

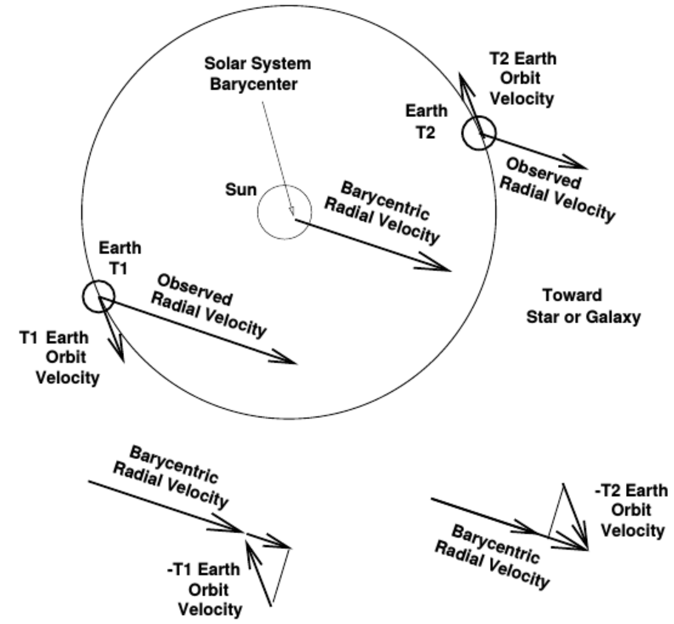

FIGURE 3.20: Correction of radial velocity observed from the earth to that which would be observed from the center of mass of teh solar system is shown at two different times in the earth's orbit, taken from the RVSAO paper!!!!!!

Chapter 4

Modelling

- C

Chapter 5

Conclusions

- Cfjsdkafdsjafkl

Bibliography

[1] Michael J. Kurtz, Douglas J. Mink. *RVSAO 2.0: Digital Redshifts and Radial Velocities*. Harvard-Smithonian Center for Astrophysics, Cambirdge, MA 02138, 1993.

[2] Roueff F., Salati P., Tillet R. *The velocity dispersion profile of globular clusters: a closer look*. preprint astro-ph/9707174v1.

[3] Binney J., Tremaine S.. *Galactic Dynamics*. Princeton University Press, 1994.